© 2019. Published by The Company of Biologists Ltd | Journal of Cell Science (2019) 132, jcs224063. doi:10.1242/jcs.224063

RESEARCH ARTICLE

Organization and function of tension-dependent complexes at adherens junctions

Cordelia Rauskolb, Estelle Cervantes, Ferralita Madere and Kenneth D. Irvine*

ABSTRACT

Adherens junctions provide attachments between neighboring epithelial cells and a physical link to the cytoskeleton, which enables them to sense and transmit forces and to initiate biomechanical signaling. Examination of the Ajuba LIM protein Jub in *Drosophila* embryos revealed that it is recruited to adherens junctions in tissues experiencing high levels of myosin activity, and that the pattern of Jub recruitment varies depending upon how tension is organized. In cells with high junctional myosin, Jub is recruited to puncta near intercellular vertices, which are distinct from Ena-containing puncta, but can overlap Vinc-containing puncta. We identify roles for Jub in modulating tension and cellular organization, which are shared with the cytohesin Step, and the cytohesin adapter Sstn, and show that Jub and Sstn together recruit Step to adherens junctions under tension. Our observations establish Jub as a reporter of tension experienced at adherens junctions, and identify distinct types of tension-dependent and tension-independent junctional complexes. They also identify a role for Jub in mediating a feedback loop that modulates the distribution of tension and cellular organization in epithelia.

KEY WORDS: Mechanotransduction, Tension, Morphogenesis, Ajuba

INTRODUCTION

Mechanical forces experienced by cells can influence the shapes of individual cells, and the structures of tissues to which they contribute (Heer and Martin, 2017). Additionally, through mechanotransduction, forces perceived by cells can be converted into biochemical responses that modulate cell behaviors. Adherens junctions (AJs) are potential sites of mechanotransduction, as they physically connect epithelial cells to each other and attach to the actin cytoskeleton, which can exert tension on AJs (Leckband and de Rooij, 2014; Lecuit and Yap, 2015; Yap et al., 2017). Proteins have been identified that are recruited to AJs under tension, including Vinculin (Vinc), Ajuba family proteins and Zyxin family proteins, but our understanding of the full complement of proteins recruited to AJs under tension, their relationships and the biological consequences of their recruitment remain incomplete.

Core AJ proteins include the transmembrane cell adhesion protein E-cadherin (E-cad; also known as Shg) and the catenins, which are associated with or linked to the E-cad cytoplasmic domain (Harris and Tepass, 2010). AJs are directly linked to the cytoskeleton through the association of α-catenin with F-actin, although they can also be linked through other AJ-associated proteins, including Vinc. α-catenin plays a key role in mechanotransduction at AJs, as it can undergo a tension-dependent conformational change that enables it to recruit Vinc (Kim et al., 2015; Yao et al., 2014; Yonemura et al., 2010), which may help to strengthen junctions under tension.

Tension-dependent recruitment of the *Drosophila* Ajuba LIM protein (Jub) or its mammalian homolog, LIMD1, to AJs has a key role in biomechanical regulation of the Hippo signaling network (Ibar et al., 2018; Rauskolb et al., 2014). Jub or LIMD1 can bind to and inhibit key kinases involved in Hippo signaling (the *Drosophila* Warts or mammalian LATS1 and LATS2 kinases) (Das Thakur et al., 2010; Rauskolb et al., 2011). Recruitment of these Ajuba family proteins to AJs requires α-catenin (Ibar et al., 2018; Marie et al., 2003; Rauskolb et al., 2014). Studies in cultured mammalian cells revealed that recruitment of Ajuba family proteins occurs at sites where, based upon binding of the a18 monoclonal antibody, and colocalization of vinculin, tension-mediated conformational changes in α-catenin occur (Ibar et al., 2018). Studies in *Drosophila* have found, however, that Vinc and Jub actually associate with distinct domains of α-catenin (Alégot et al., 2019).

Jub and LIMD1 are members of the Ajuba family of LIM domain proteins, which are characterized structurally by the presence of three LIM domains in their C-terminal halves (Schimizzi and Longmore, 2015). The Ajuba proteins are structurally related to the Zyxin proteins, which also contain three C-terminal LIM domains (Koch et al., 2012). In mammalian cells, zyxin contributes to repair of actin stress fibers (Smith et al., 2010), and it is recruited to actin stress fibers experiencing strain (Smith et al., 2013; Uemura et al., 2011), which might account for a reported tension-dependent localization to AJs (Oldenburg et al., 2015). Ajuba family proteins have been ascribed a wide range of functions, possibly reflecting a core role as scaffolding proteins, including effects on transcription, intercellular signaling pathways, microRNA processing and the cytoskeleton (Schimizzi and Longmore, 2015). They have also been ascribed a correspondingly wide range of cellular locations. However, aside from their influence on Hippo signaling, most studies have not linked Ajuba family proteins to mechanotransduction. An exception to this is the tension-dependent recruitment of the mammalian Ajuba family protein WTIP in *Xenopus*, which has been linked to apical constriction (Chu et al., 2018).

Here, we describe investigations of the recruitment and role of Jub at AJs under tension. We show that Jub can be recruited to AJs in a wide range of *Drosophila* tissues, and that the pattern of Jub recruitment varies depending on how tension is organized in different cell types. We compare Jub recruitment to other proteins recruited to a subset of AJs and thereby identify distinct AJ-associated complexes in *Drosophila* cells. We characterize Hippo-independent Jub phenotypes, and establish a mechanistic basis for them by showing that Jub is responsible, together with Stepping stone (Sstn), for a tension-dependent recruitment of the cytohesin Steppke (Step) to AJs, which then modulates myosin

Waksman Institute and Department of Molecular Biology and Biochemistry, Rutgers University, Piscataway, NJ 08854, USA.

*Author for correspondence (Irvine@waksman.rutgers.edu)

F.M., 0000-0001-7710-3444; K.D.I., 0000-0002-0515-3562

Received 17 August 2018; Accepted 22 February 2019

Journal of Cell Science (2019) 132, jcs224063. doi:10.1242/jcs.224063

distribution and cellular organization. These observations implicate Jub as a key component of a negative-feedback loop that stabilizes and distributes tension at AJs.

RESULTS

Recruitment of Jub to junctions in cells with elevated myosin activity

Tension-dependent recruitment of Jub to AJs was first identified in *Drosophila* wing imaginal discs, where Jub contributes to regulation of Hippo signaling (Rauskolb et al., 2014). To investigate the potential tension-dependent recruitment of Jub in other tissues, we used a Jub:GFP genomic construct (Sabino et al., 2011) to examine Jub localization in *Drosophila* embryos. This revealed that Jub is detected at AJs throughout embryonic development, and that Jub levels at junctions are elevated in cells known to have high actomyosin contractility (Heer and Martin, 2017; Martin and Goldstein, 2014; Tamada and Zallen, 2015), including in ventral furrow and posterior midgut cells undergoing apical constriction, in cells of the developing pharynx, and in leading-edge and amnioserosa cells during dorsal closure (Fig. 1A–C,E; Fig. S1A,B). We also observed that, along junctions where Jub recruitment is relatively low, it could be increased by increasing myosin activity (Fig. S1B,C), as in imaginal discs (Rauskolb et al., 2014) and as for mammalian Ajuba family proteins (Chu et al., 2018; Ibar et al., 2018). Tension-dependent recruitment of Jub to AJs in embryonic epithelia was also recently noted by Razzell et al. (2018). Thus, robust recruitment of Jub to AJs appears to be a general feature of epithelial cells experiencing high levels of actomyosin contractility.

Spatial organization of myosin influences Jub recruitment to junctions

In wing discs, the Jub distribution includes both a low-level, relatively uniform accumulation along cell–cell junctions and a discrete high-level accumulation in puncta that occur preferentially near intercellular vertices (Figs 1D and 2A; Fig. S1D,E) (Rauskolb et al., 2014). The precise location of Jub puncta varies, however, such that when Jub intensities along many junctions are averaged, its distribution is only slightly different from that of E-cad (Fig. S1E). Jub puncta are more numerous along compartment boundaries, where myosin accumulation and junctional tension are higher (Rauskolb et al., 2014). In embryos, distinct Jub distributions are visible in different cell types. Most epidermal cells exhibit a Jub distribution similar to that in wing discs – a low-level junctional accumulation, plus brighter puncta that are often near vertices (Fig. 1; Fig. S1). In contrast, cells with high levels of apical-medial myosin and undergoing apical constriction have relatively high levels of Jub at junctions around the entire cell circumference. Cells exhibiting this circumferential distribution of elevated Jub include ventral furrow and posterior midgut cells (Fig. 1A; Fig. S1A), which undergo apical constriction that contributes to their invagination, and amnioserosa cells (Figs 1B,E and 2C), which undergo a constriction that pulls lateral epidermal cells dorsally, thus driving dorsal closure (Heer and Martin, 2017; Martin and Goldstein, 2014).

A particularly informative Jub distribution is observed near the dorsal side of the leading-edge cells (where dorsal epidermal cells contact the amnioserosa). A multicellular actomyosin cable here establishes tension that surrounds the amnioserosa and contributes to efficient dorsal closure (Franke et al., 2005). In the leading-edge cells, bright puncta of Jub accumulation are observed near the junctions between leading-edge cells, in line with the actomyosin cable and adjacent to the peak myosin levels that occur between the junctions (Figs 1B,E and 2C; Fig. S1B,F). These accumulations could sometimes be resolved into two nearby puncta, one on each side of the cell–cell junction (Fig. 2C; Fig. S1F). Jub puncta often appear to have a diameter close to the diffraction limit (~250 nm; Fig. 2C). The distinct Jub localization in different cell types indicates that Jub distribution is influenced both by the amount of tension in a cell, and also by how that tension is organized.

Distinct AJ complexes in *Drosophila* epithelia

The conclusion that α-catenin undergoes a tension-dependent conformational change was based, in part, on investigations of binding between α-catenin and vinculin in mammalian cells (Kim et al., 2015; Yao et al., 2014; Yonemura et al., 2010). In *Drosophila*, Vinc localization can be detected using genomic GFP- or RFP-tagged transgenes (Klapholz et al., 2015). In wing disc cells, we observed extensive colocalization between Jub and Vinc, as – in most cases – bright puncta of localization at junctions coincide (Fig. 2A,B; Fig. S1E,F), consistent with the suggestion that they are recruited to junctions through a shared process. Quantification of colocalization, by calculation of Pearson's colocalization coefficient, identified partial colocalization between Jub and Vinc in wing discs (Fig. S2D). Moreover, we confirmed that junctional localization of Vinc in wing discs is tension dependent, as it was reduced by RNA interference (RNAi) targeting the myosin activator Rho kinase (Rok) and enhanced by expression of an activated form of myosin light chain (Sqh.EE) (Fig. 2G; Fig. S2A,B). It has also been reported that Vinc localization to junctions within embryos can be promoted by increased tension (Jurado et al., 2016; Kale et al., 2018). We also compared Vinc to Jub localization in leading-edge cells during dorsal closure, but observed only partial overlap between Jub and Vinc (Fig. S2C,D), suggesting that additional mechanisms contribute to Vinc recruitment in these cells.

The punctate localization of Jub and Vinc in wing discs marks a distinct type of AJ that is promoted by cytoskeletal tension. Several other proteins have been reported to exhibit a punctate distribution along AJs; hence, we examined whether they colocalize with Jub, or instead identify different protein complexes. Enabled (Ena) is an actin regulator homologous to mammalian VASP proteins and accumulates in puncta near intercellular vertices, both in wing discs and in leading-edge cells (Gates et al., 2007; Major and Irvine, 2005). However, Ena puncta, examined using anti-Ena antibodies, are usually adjacent to, rather than overlapping, Jub puncta (Fig. 2B–D; Fig. S2E). Quantification of colocalization in wing discs confirms significantly less overlap of Ena with Jub, compared to Vinc (Fig. S2D). Quantification of the mean distribution along junctions revealed that Ena puncta tend to be closer to tricellular vertices than Jub puncta in wing discs, and that Ena is less evenly distributed along junctions, i.e. peaks associated with Ena puncta are more prominent when junctional distributions are averaged (Fig. S2I,J). Along the leading edge, where the rectangular organization of cell–cell junctions facilitates direct comparisons, Jub puncta are consistently closer to cell–cell junctions than Ena puncta (Fig. 2C; Figs S1F and S2E). Vinc puncta were also clearly distinct from Ena puncta in wing discs (Fig. 2B; Fig. S2G), but partially overlapping in leading-edge cells (Fig. S2F), consistent with the observed relationship between Jub and Vinc.

Drosophila Zyxin (Zyx) also exhibits a punctate distribution in disc epithelial cells (Rauskolb et al., 2011). Zyx can interact with Ena/VASP proteins (Drees et al., 2000; Gaspar et al., 2015). Comparisons of the Zyx distribution to that of Ena, using a UAS-YPet:Zyx transgene, revealed extensive colocalization (Fig. 2E; Fig. S2G,H). Certain antibodies that recognize phosphorylated tyrosine, including the anti-p-Tyr monoclonal PY20, and antisera

Journal of Cell Science (2019) 132, jcs224063. doi:10.1242/jcs.224063

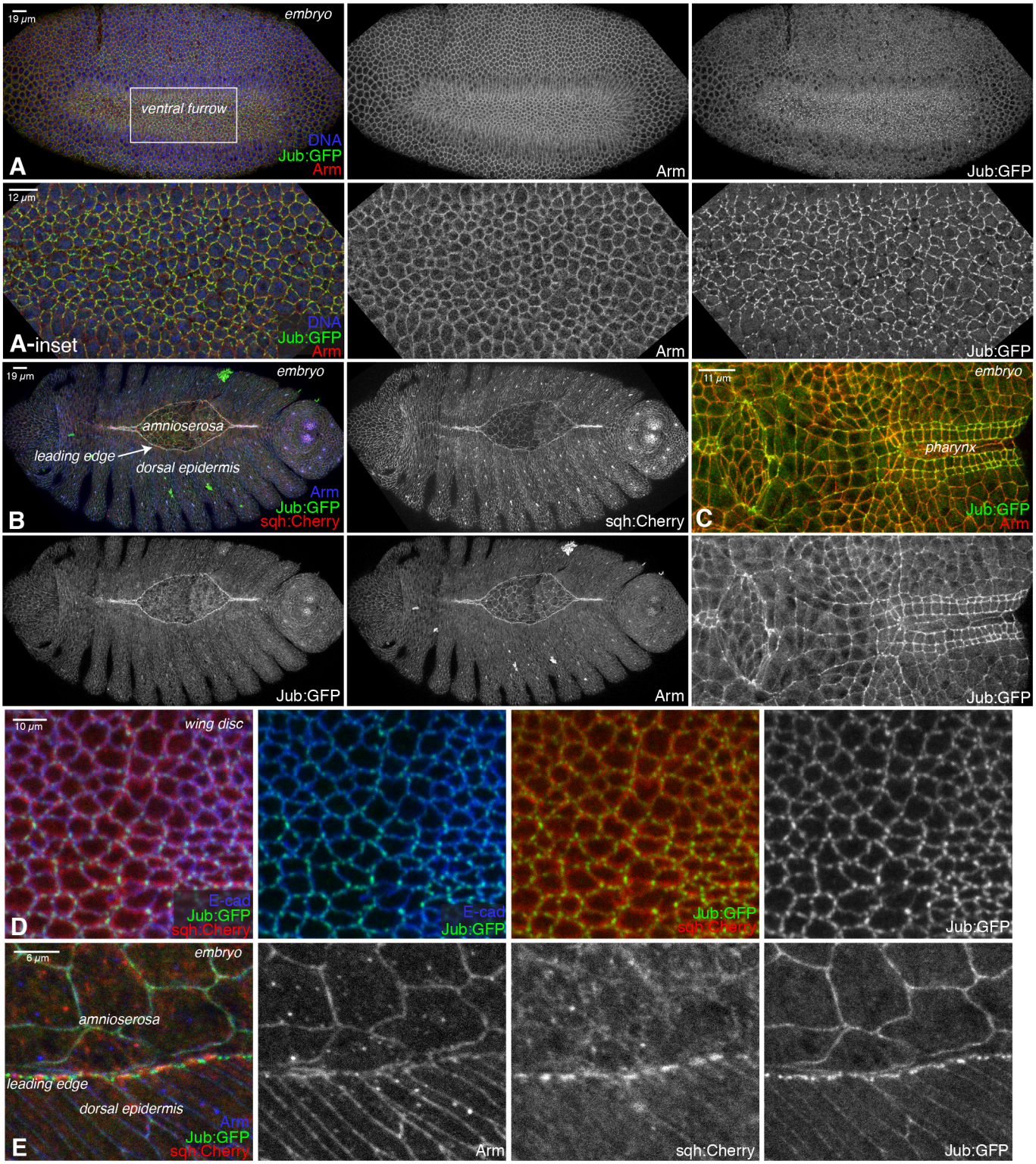

Fig. 1. Jub localization at different stages of development. (A–E) Localization of Jub:GFP (green/white) in ventral furrow, compared to DNA (blue) and Armadillo (Arm, β-catenin, red/white) (A); dorsal closure, compared to Arm (blue/white) and Sqh:Cherry (red/white) (B); pharynx, compared to Arm (red) (C); wing disc, compared to Sqh:Cherry (red) and E-cad (blue) (D); and dorsal closure, compared to Arm (blue/white) and Sqh:Cherry (red/white) (E). Scale bars are shown at the top left of images in figures. Insets show higher-magnification views of the boxed region in A.

recognizing a phosphorylated tyrosine on β-catenin (Y654), can also generate a punctate staining pattern in *Drosophila* epithelia (Brunet et al., 2013; Major and Irvine, 2005). Although β-cat-pY654 staining exhibits a broader distribution than YPet:Zyx or Ena staining, the most intense puncta of β-cat-pY654 overlap with YPet:Zyx and Ena (Fig. S2G,H).

Another distinct type of junctional complex was identified by localization of the Sidekick (Sdk) protein. Sdk is an immunoglobulin

Journal of Cell Science

Journal of Cell Science (2019) 132, jcs224063. doi:10.1242/jcs.224063

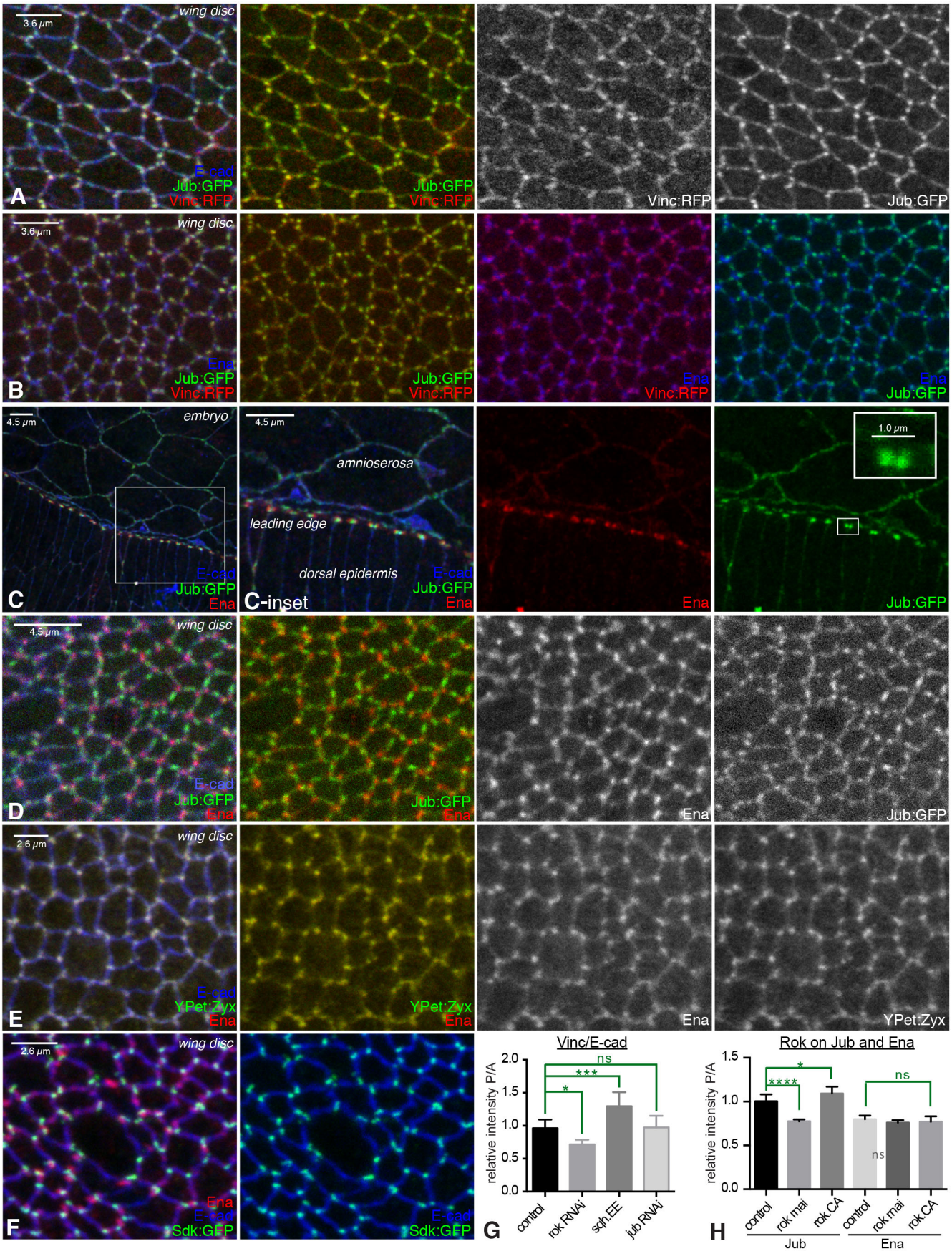

Fig. 2. See next page for legend.

Journal of Cell Science (2019) 132, jcs224063. doi:10.1242/jcs.224063

Fig. 2. Colocalization of AJ complex proteins. (A–F) Examination of colocalization amongst proteins in AJ complexes, with AJs marked by E-cad (blue). Portions of wing discs are shown in A, B and D–F; C shows the leading edge during dorsal closure. (A) Jub:GFP (green/white) overlaps Vinc:RFP (red/white). (B) Jub:GFP (green) and Vinc:RFP (red) overlap each other, but do not overlap Ena (blue). (C) Ena (red) puncta are adjacent to Jub (green) puncta in leading-edge cells; Jub puncta are closer to leading-edge cell–cell junctions. Insets show higher-magnification views of the boxed regions. (D) Jub (green/white) puncta do not overlap Ena (red/white) puncta. (E) Ena (red/white) puncta overlap YPet:Zyx (green/white) puncta. (F) Sdk:GFP (green) overlaps E-cad (blue) but not Ena (red). (G) Quantification of the relative junctional intensity of Vinc, normalized to E-cad intensity, in posterior (P) versus anterior (A) cells in wing discs expressing control UAS line (n=14), *UAS-Rok* RNAi (n=5), *UAS-sqh.EE* (n=8) or *UAS-jub* RNAi (n=13) under *en-Gal4* control. (H) Quantification of the relative junctional intensity of Jub and Ena, as indicated, in P versus A cells in wing discs expressing control UAS line (n=7), *UAS-Rok* RNAi (n=14) or *UAS-Rok.CA* (n=6) under *en-Gal4* control. For G and H, significant differences from control are indicated. ns, not significant; $P>0.05$; *$P\leq0.05$, ***$P\leq0.001$, ****$P\leq0.0001$. Error bars indicate 95% c.i.

superfamily protein that has been studied for its role in the nervous system (Nguyen et al., 1997), but has also been reported to exhibit a punctate distribution in epithelia (Lye et al., 2014). Examination of Sdk localization using an Sdk:GFP protein trap revealed that it consistently localizes directly at intercellular vertices (Fig. 2F; Fig. S2J), which distinguishes it from the more variable near-vertices localization of Ena or Jub. Sdk is also distinct from the previously described *Drosophila* tricellular vertices proteins Bark beetle and Gliotactin (Byri et al., 2015; Schulte et al., 2003), as they overlap with septate junctions proteins, whereas Sdk overlaps with E-cad (Fig. 2F). Altogether, our localization studies suggest that a single wing disc cell has at least four different types of AJ complexes: Jub-associated, Ena-associated, Sdk-associated, and AJs lacking Jub, Ena and Sdk complexes.

The Jub complex is regulated by tension (Rauskolb et al., 2014). To investigate whether Ena localization is influenced by tension, we examined the consequences of either decreasing or increasing tension. Tension was decreased in posterior wing disc cells by *en-Gal4*-driven RNAi of Rok or increased by expression of activated Rok (Rok.CA). Ena levels at junctions are normally slightly lower in posterior wing disc cells than in anterior wing disc cells (Fig. 2H; Fig. S3C) (Gaspar et al., 2015). Decreasing tension in posterior cells mildly decreased Ena localization at junctions in posterior cells, but the decrease was not significant (Fig. 2H; Fig. S3A). Moreover, increasing tension did not increase Ena localization at junctions, in contrast to the increase in Jub recruitment (Fig. 2H; Fig. S3B). These observations suggest that Ena does not directly respond to tension on junctions.

Independent recruitment of proteins to AJ complexes

To investigate functional relationships among proteins in the Jub- and Ena-containing complexes, we used RNAi to knock down the expression of complex components, and then examined whether the localization of other proteins was affected. RNAi lines were expressed in posterior cells under an *en-Gal4* driver, such that anterior cells could be used as an internal control for protein localization and staining. The effectiveness of the RNAi lines was confirmed by fluorescence imaging (Fig. S4). This analysis suggested that Jub and Vinc are each independently recruited to AJs in wing disc cells, as Vinc was still recruited to AJs in *jub* RNAi cells, and Jub was still recruited to AJs in *Vinc* RNAi cells (Figs 2G and 3A,B,F).

We also assayed for potential interactions between complexes by examining Ena localization in cells subject to RNAi for *jub* or *Vinc*, and Jub localization in cells subject to RNAi for *ena* or *Zyx*. Ena localization was not visibly affected by knockdown of *jub* or *Vinc*, or knockdown of *Zyx* (Fig. 3C,E,G,H; Fig. S3D), consistent with the detection of junctional Ena in *Zyx* mutants (Gaspar et al., 2015). Jub localization was similarly unaffected by knockdown of *ena* (Fig. 3D,F), although, unexpectedly, Jub levels at junctions were reduced by knockdown of *Zyx* (Fig. 3E,F). Zyx localization was not obviously affected by knockdown of *ena* or *jub* (Fig. 3I; Fig. S3F–H). Thus, with the exception of an influence of Zyx on Jub localization, it appears, based on the level of knockdown achieved using RNAi, that each of these proteins localizes to AJ complexes independently.

Influence of Jub on cellular organization

The widespread accumulation of Jub at AJs throughout embryogenesis, often in cell types in which Hippo signaling has no known role, raised the question of whether Jub might have other functions at AJs. Indeed, mammalian homologs of Jub have been ascribed a range of activities in addition to their influence on Hippo signaling, including effects on transcriptional repression, centrosome integrity, microRNA processing and cell adhesion (Schimizzi and Longmore, 2015). To begin to investigate potential functions in *Drosophila* embryos, we examined *jub* mutant embryos, using a previously described null allele (Das Thakur et al., 2010), but observed no evident defects. As *jub* might also be maternally contributed, we then created and examined *jub* mutant embryos derived from *jub* mutant germline clones (henceforth, *jub* embryos). Less than 10% of *jub* embryos die during embryogenesis (Fig. S5B); most die during larval stages and none survive to adulthood. Examination of larval cuticles did not reveal any consistent defects associated with *jub* embryos. To further investigate potential developmental defects in *jub* embryos, we focused on dorsal closure, because of the prominent elevation of Jub at junctions in cells known to contribute to dorsal closure, and because dorsal closure is a key morphogenetic event during embryogenesis that depends upon actomyosin contractility (Franke et al., 2005; Martin and Goldstein, 2014).

Both examination of fixed embryos and time-lapse imaging of live embryos revealed that dorsal closure still occurs in *jub* embryos, which is consistent with the absence of defects in the dorsal cuticle of *jub* embryos and larvae. However, examination of individual cells using anti-E-cad staining, or an E-cad:GFP transgene, revealed differences in cellular organization in the dorsal and lateral epidermis. In wild-type embryos, these cells become elongated and organized into rows perpendicular to the leading edge as they are stretched by the contracting amnioserosa (Fig. 4A; Movie 1). Most of these wild-type cells have a similar size, and a similar, nearly rectangular, shape. In *jub* embryos, by contrast, there is greater heterogeneity in cell sizes, shapes and arrangements (Fig. 4B,C; Movie 2). One notable aspect of the altered cellular shapes and arrangements is an increase in multicellular rosettes, defined as five or more cells sharing a common intercellular vertex. Rosettes contribute to cellular rearrangements that drive germband extension (Blankenship et al., 2006). They can also occur during dorsal closure, but, during this process, are normally rare and transient (West et al., 2017). However, both the frequency and duration of rosettes was substantially increased in *jub* embryos compared to wild-type embryos (Fig. 4A–E). In addition to altered cellular organization, in a fraction of embryos (<20%), gaps occur within the amnioserosa, particularly at the junction between the amnioserosa and leading-edge cells (Fig. 4F), or within the actin cable along the leading edge (Fig. S5A). The defects observed in *jub*

Journal of Cell Science (2019) 132, jcs224063. doi:10.1242/jcs.224063

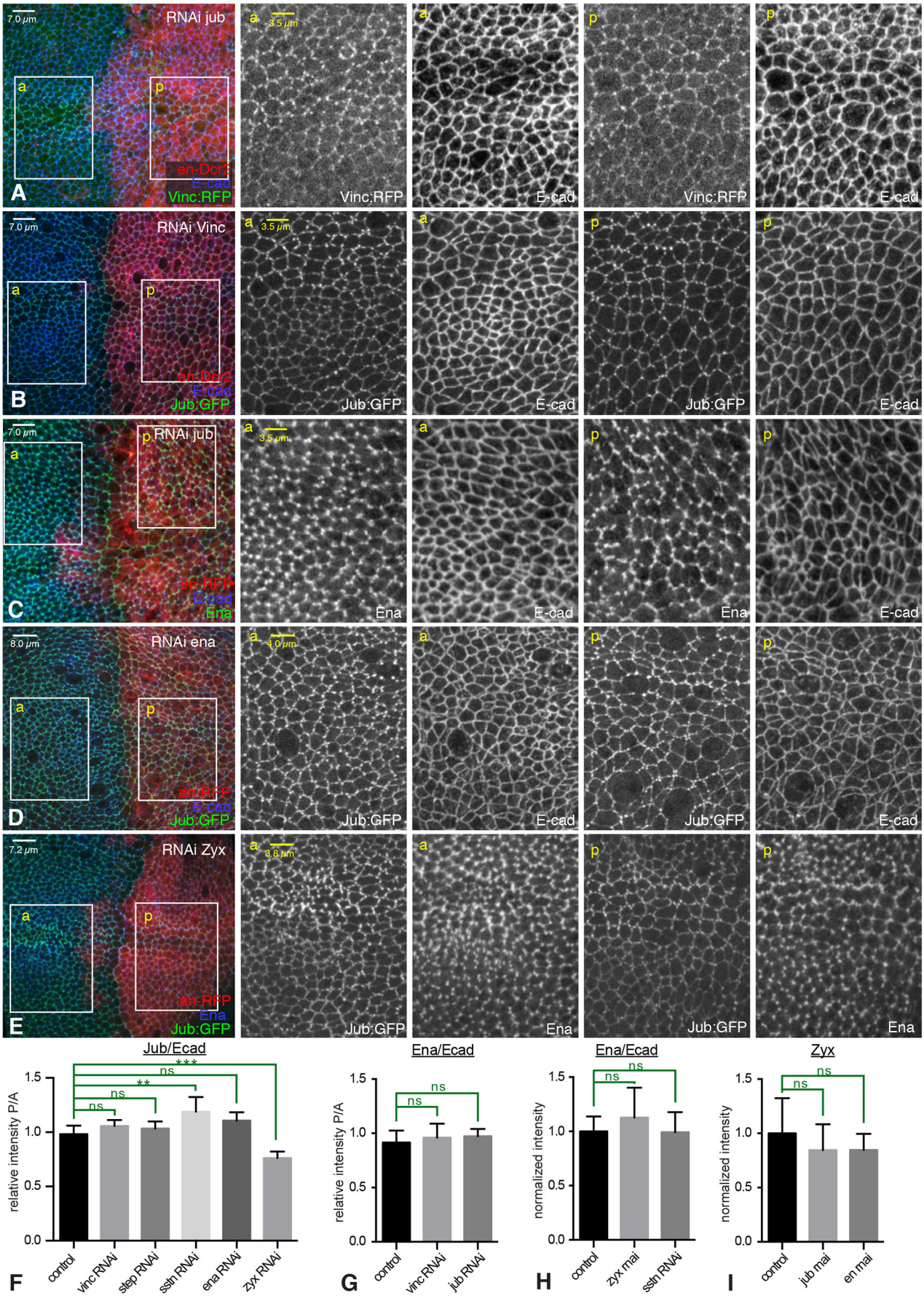

Fig. 3. See next page for legend.

Journal of Cell Science

Journal of Cell Science (2019) 132, jcs224063. doi:10.1242/jcs.224063

Fig. 3. Independent junctional localization of AJ proteins. (A–E) Leftmost column: wing imaginal discs in which UAS-RNAi lines were expressed in posterior cells (red) under *en-Gal4* control to assess potential requirements for localization of AJ complex proteins, with AJs marked by E-cad staining (blue/white). Columns to the right show higher-magnification views of the anterior (a) or posterior (p) boxes. (A) RNAi of *jub* does not affect Vinc (green/white) localization. (B) RNAi of *Vinc* does not affect Jub (green/white) localization. (C) RNAi of *jub* does not affect Ena (green/white) localization. (D) RNAi of *ena* does not affect Jub (green/white) localization. (E) RNAi of *Zyx* slightly decreases Jub (green/white) localization and does not affect Ena (blue/white). (F) Quantification of the relative junctional intensity of Jub, normalized to E-cad intensity, in P versus A cells in wing discs expressing control UAS line (n=12), *UAS-Vinc* RNAi (n=8), *UAS-step* RNAi (n=9), *UAS-sstn* RNAi (n=7), *UAS-ena* RNAi (n=6) or *UAS-zyx* RNAi (n=6) under *en-Gal4* control. (G) Quantification of the relative junctional intensity of Ena, normalized to E-cad intensity, in P versus A cells in wing discs expressing control UAS line (n=8), *UAS-Vinc* RNAi (n=5) or *UAS-jub* RNAi (n=10) under *en-Gal4* control. (H) Quantification of the relative junctional intensity of Ena, normalized to E-cad intensity, in wing discs expressing control UAS line (n=21), *UAS-Zyx* RNAi (n=12) or *UAS-sstn* RNAi (n=14) under *nub-Gal4* control, normalized to the mean intensity ratio in control discs. (I) Quantification of the relative junctional intensity of Zyx in wing discs expressing *UAS-YPet:Zyx* and control UAS line (n=7), *UAS-jub* RNAi (n=6), or *UAS-ena* RNAi (n=8) under *en-Gal4* control, normalized to the mean intensity in control discs. Significant differences from control are indicated; ns, not significant; $P>0.05$; $^{**}P\leq0.01$, $^{***}P\leq0.001$. Error bars indicate 95% c.i.

embryos during dorsal closure have some similarities to defects observed in *ena*, *canoe* (*cno*) or *polychaetoid* (*pyd*) mutant embryos (Choi et al., 2011; Gates et al., 2007). However, those mutants have reduced embryonic viability compared to *jub* embryos and also exhibit additional defects, including failures in head involution and retraction of segmental grooves, which were not observed in *jub* embryos.

jub and *step* exhibit similar phenotypes

The defects in cellular organization observed during dorsal closure, particularly the increased number and duration of multicellular rosettes, are reminiscent of the phenotype of *step* mutant embryos (West et al., 2017). Step is the *Drosophila* cytohesin, a guanine-nucleotide exchange factor (GEF) for Arf family G proteins (Jackson and Bouvet, 2014). Step has been implicated in several different biological processes, including receptor tyrosine kinase signaling, endocytic regulation and cytoskeletal regulation (Donaldson and Jackson, 2011; Jackson and Bouvet, 2014). Recently, Step was implicated in a negative-feedback loop that reduces tension within dorsal epidermal cells, thus facilitating their stretching and elongation in response to external tension provided by constriction of the amnioserosa (West et al., 2017). This suggestion was based, in part, on observations that Step localization to cell junctions is promoted by cytoskeletal tension and experiments suggesting that tissue tension is higher in *step* mutant embryos.

To begin to investigate the possibility that Jub and Step activities are connected, we compared their localization, using a *UAS-step:Cherry* transgene (Lee and Harris, 2013). This revealed colocalization between Jub and Step at multiple sites, including puncta along the leading edge during dorsal closure, puncta near vertices in dorsal epidermal cells and puncta in wing imaginal disc cells (Fig. 4G,H; Fig. S2D).

To assess the potential significance of their colocalization in wing imaginal discs, we compared the phenotypes of wing discs in which *jub* or *step* were knocked down in posterior cells by *en-Gal4* driven RNAi. This revealed defects in both cellular organization and myosin accumulation (Fig. 5A–C; Fig. S6A–C). Examination of E-cad staining revealed increased heterogeneity of cell shapes and sizes. The myosin distribution in wing discs was also strikingly abnormal. Normally, most cell–cell junctions in the wing disc have similar levels of myosin accumulation. Conversely, in regions depleted of *jub* or *step*, prominent multicellular cables with elevated myosin were detected, but, at the same time, myosin levels were greatly reduced or even undetectable on other cell junctions (Fig. 5; Fig. S6). The influence of *jub* and *step* on myosin was similar, but, in contrast to *jub* RNAi, *step* RNAi did not significantly reduce the size of the posterior compartment, suggesting that, unlike Jub, Step does not promote Yki activity. To confirm this, we also examined the influence of *step* RNAi on expression of a Yki target gene, *expanded* (*ex*), and on wing size. Overall wing size is only modestly reduced by *step* RNAi (Fig. S5E,G), and expression of an *ex* reporter gene, *ex-lacZ*, was not visibly affected (Fig. S5J). Further evidence that the reorganization of myosin in *jub* or *step* knockdown cells is unrelated to Hippo signaling was provided by comparisons to *Zyx*, which has effects similar to *jub* on Hippo signaling (Rauskolb et al., 2011), but not on myosin distribution (Fig. 5E; Fig. S6E).

Jub and Sstn cooperate to promote Step localization to AJs

To investigate the possibility that the shared phenotypes and colocalization of Jub and Step stem from a direct connection between them, we asked whether knockdown of either protein influenced the localization of the other. As Step localization was assessed using UAS transgenes, we used *nub-Gal4* to drive *UAS-step:Cherry* and RNAi line expression throughout the wing pouch to assay for effects on Step localization (*UAS-step* is lethal in combination with *en-Gal4*). As we lack antisera against Step protein, the effectiveness of *step* RNAi was confirmed by its ability to knock down levels of Step:Cherry (Fig. S4I,J). We observed an apparent hierarchical relationship between Jub and Step: Jub knockdown was sufficient to remove Step from AJs (Fig. 6A,B,F), but Step knockdown was not sufficient to remove Jub from AJs (Fig. 3F; Fig. S7A). As a control, we confirmed that Step localization to AJs is still detected in *Zyx* RNAi wings discs (Fig. 6F; Fig. S7C). Jub localization is slightly altered in *step* RNAi wing discs, as lines of elevated Jub puncta are detected (Fig. S7A), which is consistent with the reorganization of myosin induced by loss of Step (Fig. 5C; Fig. S6C).

Sstn was identified as an adapter protein that contributes to Step localization at membranes during cellularization of *Drosophila* embryos (Liu et al., 2015). We thus extended our analysis to Sstn using *UAS-sstn:Cherry* or *UAS-sstn:GFP* transgenes, and *sstn* RNAi (Fig. S4K,L). Sstn also colocalizes with Jub at AJs in wing disc cells (Fig. 4I; Fig. S2D). The colocalization of Step and Sstn with Jub suggested that their junctional localization might also be promoted by tension. To examine this, we reduced tension in wing discs expressing GFP-tagged Step or Sstn by RNAi of *Rok*. This resulted in a strong and consistent decrease in junctional recruitment of Step (Fig. 6G; Fig. S7D,E), but a weaker and more variable decrease in Sstn recruitment, which was not statistically significant (Fig. 6H; Fig. S7F,G).

To assess the functional significance of Sstn colocalization, we examined *sstn* RNAi in wing discs. This results in a phenotype similar to *jub* or *step* knockdown, including intercellular cables with elevated myosin along some junctions and absent myosin along other junctions, as well as irregular cell shapes and sizes (Fig. 5D; Fig. S6D). Sstn was not required for wing growth or Yki activity (Fig. S5F,G,K). Knockdown of *sstn* also revealed that it is required for Step localization to AJs in wing disc cells (Fig. 6C,F), which could thus account for the *sstn* wing disc phenotype. Conversely, knockdown of Sstn did not prevent Jub localization to AJ (Fig. 3F;

Journal of Cell Science (2019) 132, jcs224063. doi:10.1242/jcs.224063

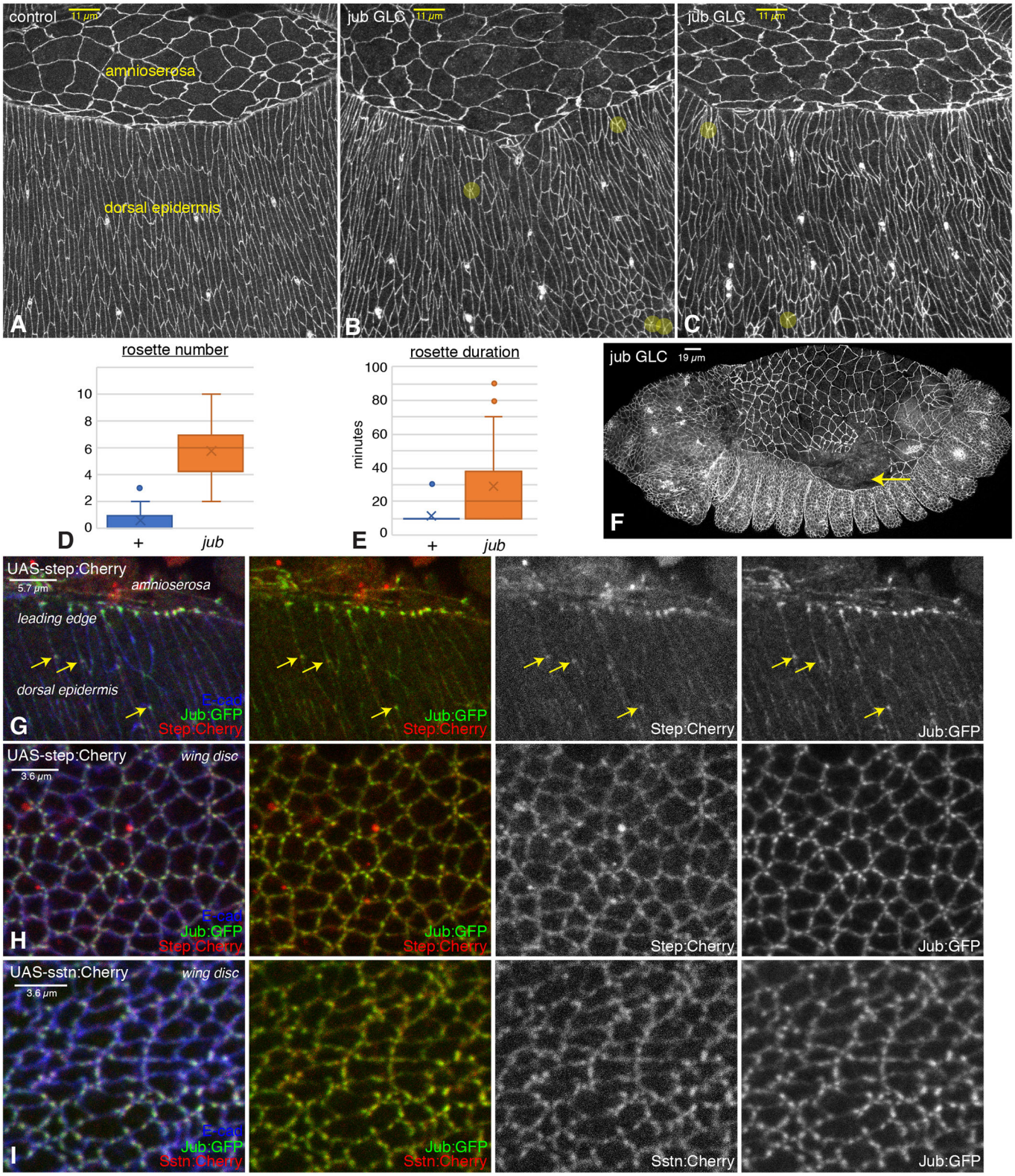

Fig. 4. Embryonic phenotypes of *jub* and colocalization with Step. (A–C) Dorsal epidermal cells of wild-type (A) and *jub* germ line clone (B,C) embryos. Examples of rosettes are marked by yellow circles. (D,E) Quantification of average rosette number per half embryo at each time point (D) and duration of rosettes (E) from live embryos imaged every 10 min during the last 2 h of dorsal closure displayed as a Tukey box plot, with X marking the mean. (F) Example of *jub* embryo with detachment of amnioserosa from the leading edge (arrow). (G) Colocalization of Jub (green/white) with Step (red/white) in the dorsal epidermis and leading-edge cells of embryos expressing *UAS-step:Cherry* under *da-Gal4* and *act-Gal4* control. Arrows highlight examples of Jub and Step colocalization in the dorsal epidermis. (H) Colocalization of Jub (green) with Step (red) in wing disc cells expressing *UAS-step:Cherry* under *nub-Gal4* control. (I) Colocalization of Jub (green) with Sstn (red) in wing disc cells expressing *UAS-sstn:Cherry* under *nub-Gal4* control.

Journal of Cell Science (2019) 132, jcs224063. doi:10.1242/jcs.224063

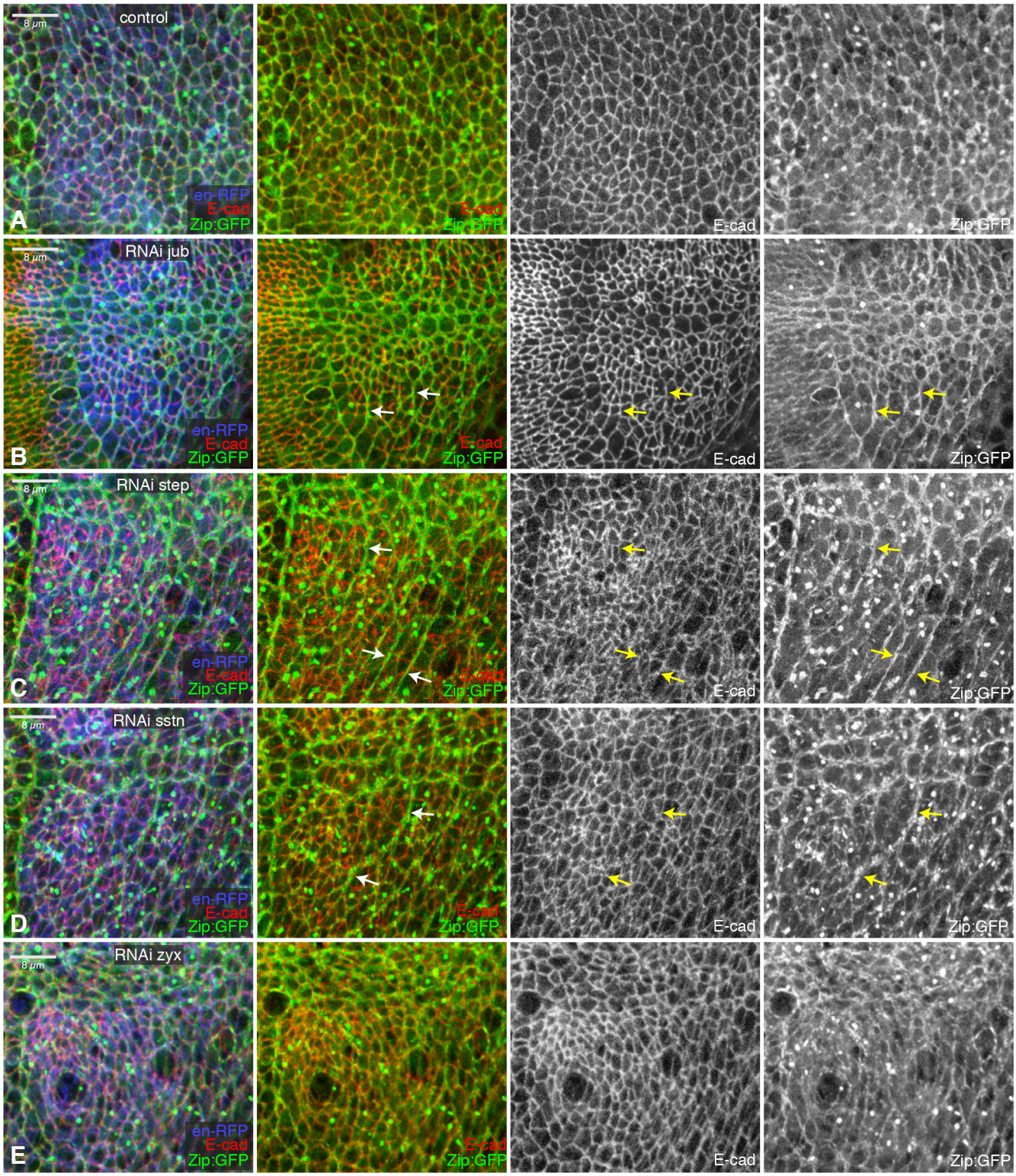

Fig. 5. Influence of *jub*, *step* and *sstn* on wing disc epithelia. (A–E) Close-ups of wing discs expressing RNAi lines in posterior cells (marked by UAS-RFP, blue) under *en-Gal4* control, stained for E-cad (red/white) and also expressing Zip:GFP (green/white) and control (A), UAS-jub RNAi (B), UAS-step RNAi (C), UAS-sstn RNAi (D) or UAS-Zyx RNAi (E). Arrows point to examples of myosin cables that extend across multiple cells.

Fig. S7B), nor did knockdown of Jub prevent Sstn localization to AJ (Fig. 6D,E,H). Thus, based on the levels of knockdown that could be achieved by RNAi, it appears that Sstn and Jub are each independently recruited to AJs, and Sstn and Jub are then both required for normal Step recruitment to AJs.

DISCUSSION

Jub levels at junctions are elevated in a wide range of cell types with elevated actomyosin contractility during embryogenesis. Together with prior studies demonstrating that myosin activity promotes junctional localization of Jub in wing disc cells (Rauskolb et al.,

Journal of Cell Science (2019) 132, jcs224063. doi:10.1242/jcs.224063

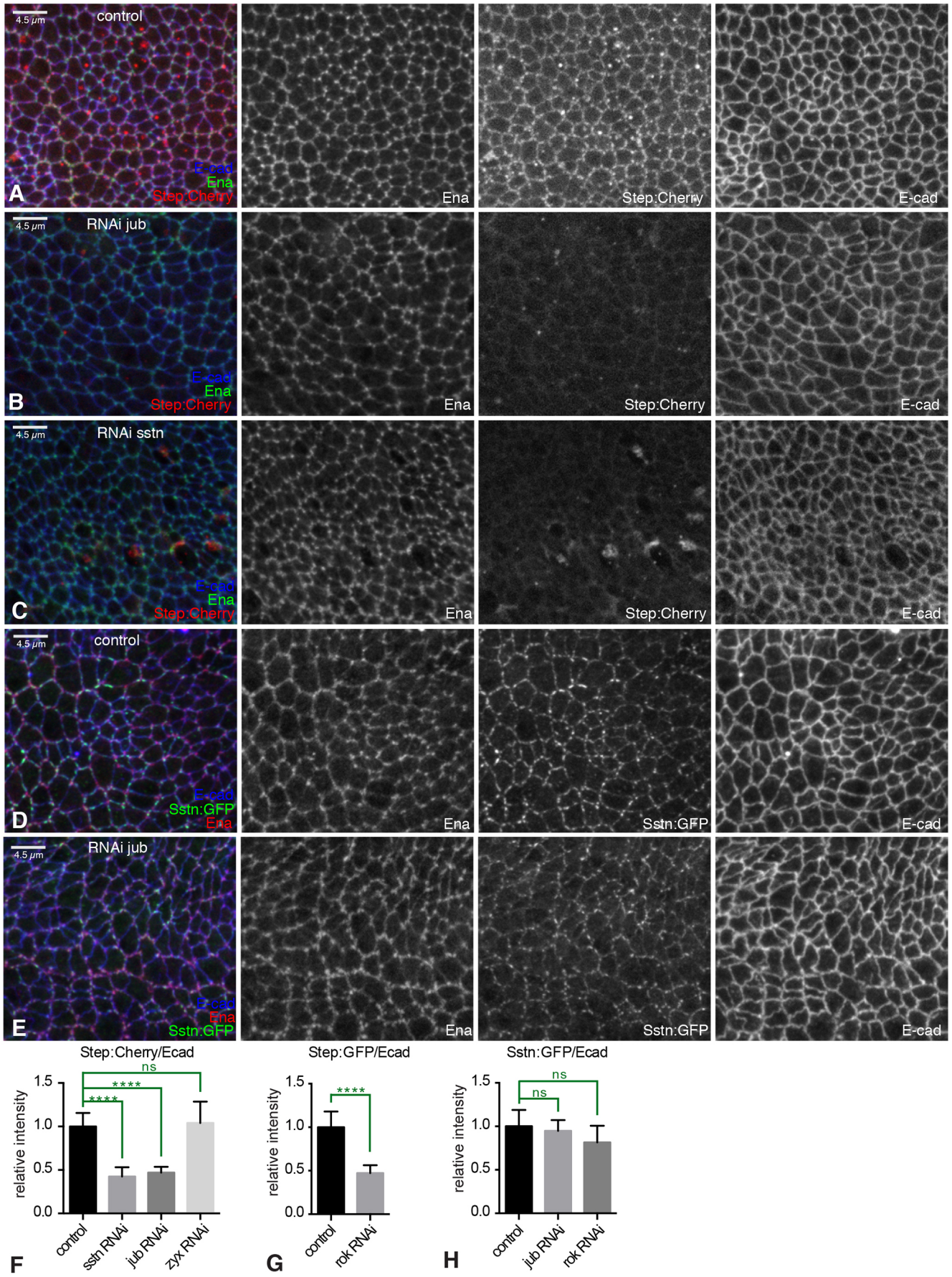

Fig. 6. See next page for legend.

Journal of Cell Science

Fig. 6. Regulation of Step localization by Jub and Sstn in wing discs. (A–E) Close-ups of control wing discs expressing *UAS-step:Cherry* or *UAS-sstn:GFP*, or wing discs also expressing UAS-RNAi lines under *nub-Gal4* control, and stained for Ena (green/red/white) and E-cad (blue/white). (A) Control disc showing localization of Step:Cherry (red/white). (B) RNAi of *jub* leads to loss of Step:Cherry (red/white) from junctions. (C) RNAi of *sstn* leads to loss of Step:Cherry (red/white) from junctions. (D) Control disc showing localization of Sstn:GFP (green/white). (E) RNAi of *jub* does not influence junctional localization of Sstn:GFP (green/white). (F) Quantification of the relative junctional intensity of Step:Cherry, normalized to E-cad intensity, in wing discs expressing control UAS line (n=20), *UAS-sstn* RNAi (n=13), *UAS-jub* RNAi (n=28) or *UAS-zyx* RNAi (n=9) under *nub-Gal4* control, normalized to the mean intensity ratio in control discs. (G) Quantification of the relative junctional intensity of Step:GFP, normalized to E-cad intensity, in wing discs expressing control UAS line (n=11) or *UAS-Rok* RNAi (n=13) under *nub-Gal4* control, normalized to the mean intensity ratio in control discs. (H) Quantification of the relative junctional intensity of Sstn:GFP, normalized to E-cad intensity, in wing discs expressing control UAS line (n=19), *UAS-jub* RNAi (n=10) or *UAS-Rok* RNAi (n=8) under *nub-Gal4* control, normalized to the mean intensity ratio in control discs. Significant differences from control are indicated; ns, not significant; P>0.05;****P≤0.0001. Error bars indicate 95% c.i.

2014), and junctional localization of mammalian Ajuba family proteins in cultured cells (Chu et al., 2018; Ibar et al., 2018), our observations establish Jub and its homologs as exhibiting a generalized recruitment to AJs under tension. Jub could thus be considered to act as a reporter or 'sensor' of junctional tension – a protein whose localization identifies sites at which AJs are under tension.

A hypothesis for the distinct Jub distributions observed in different cell types is suggested by the relationship between myosin and Jub localization, together with the model that Jub, like Vinc, is recruited to an 'open' form of α-catenin that occurs when α-catenin at molecules experience a pulling force from the actin cytoskeleton. This relationship between Jub and α-catenin conformation is supported by the overlap in localization between Jub and Vinc in both *Drosophila* and mammalian cells, as well as the overlap between Ajuba family protein localization and binding of the a18 monoclonal antibody (Ibar et al., 2018), which specifically recognizes an open form of α-catenin (Yonemura et al., 2010), and by the recent identification of mutant α-catenin constructs that constitutively recruit Jub to AJs (Alégot et al., 2019). We propose that, in cells with high levels of medial actomyosin contractility, α-catenin molecules around the entire cell circumference could experience a pulling force toward the center of the cell, generating the open form of α-catenin that binds Jub (Fig. 7A). This would explain the circumferential recruitment of Jub observed in ventral furrow cells, posterior midgut cells and amnioserosa cells. In contrast, in cells with high levels of junctional tension, we propose that generation of the open form of α-catenin depends upon their location and orientation relative to junctional actomyosin cables. At cell–cell junctions that intersect actomyosin cables, α-catenin molecules could be pulled into the open conformation by unidirectional tension from end-on attachment of these cables to AJs (Fig. 7A). This would be consistent with observations of actin cables in MDCK cells with elevated tension, which identified actin cables attached end-on to AJ complexes near tricellular junctions (Choi et al., 2016). One could thus expect rows of Jub puncta along actomyosin cables that mechanically connect multiple cells. Consistent with this, at high resolution, Jub puncta along the leading edge during dorsal closure could be resolved into two adjacent spots at each junction between leading-edge dorsal epidermal cells. Conversely, along cell membranes that run parallel to actomyosin cables, pulling forces experienced by α-catenin molecules from their attachment to F-actin could be balanced, such that there is no net pull on α-catenin away from the junctions, and α-catenin remains in a closed conformation that exhibits relatively little Jub association (Fig. 7A). Thus, our observations imply that Jub localization at junctions reflects not only the amount of cytoskeletal tension, but also its spatial organization.

Our observations also enhance appreciation of the *in vivo* complexity of AJs. Around the circumference of a single wing disc epithelial cell, we observed three different types of protein complexes overlapping E-cad (Fig. 7B). Jub-containing complexes, established by tension on AJs, are characterized by tension-dependent recruitment of Jub. They also include Warts and Step, recruited in a Jub-dependent fashion, and Vinc and Sstn, recruited independently of Jub. Ena-containing complexes are characterized by recruitment of Ena and Zyx, and also by elevated tyrosine phosphorylation of β-catenin. Jub- and Ena-containing complexes are adjacent rather than overlapping. Studies in mammalian cells have identified zyxin and vinculin as proteins that can associate with Ena/VASP proteins (Drees et al., 2000; Reinhard et al., 1999), and *Drosophila* Ena and Zyx can physically associate (Gaspar et al., 2015); but, how Ena is recruited to a complex in *Drosophila* epithelia that, at the level of confocal microscopy, overlaps or is adjacent to AJs, remains unclear. We also identified Sdk as a protein that localizes specifically to intercellular vertices. Its role there remains unknown, but we note that strong *sdk* mutants are viable (Astigarraga et al., 2018), implying that it is not essential for epithelial integrity.

Our examination of *jub* embryos led to identification of a role for Jub in controlling the organization of epithelial cells and the distribution of junctional myosin. In both dorsal epidermal cells and wing imaginal disc cells, loss of *jub* leads to changes in cellular organization. A distinctive feature of the *jub* phenotype in dorsal epidermal cells – an increased number and persistence of multicellular rosettes during dorsal closure – led us to discover a relationship between the requirement for Jub and the requirement for Step. Further analysis revealed that Jub and Step colocalize at tension-dependent puncta along AJs, that Jub is required for localization of Step at AJs, and that loss of *jub* or loss of *step* results in similar phenotypes in both embryos and wing imaginal discs. The role of Jub in recruiting Step to AJs establishes a molecular basis for this class of *jub* phenotypes.

Step is a cytohesin, a class of GEFs for Arf family G proteins. Cytohesins have been implicated in a range of different activities, including regulation of signal transduction, endocytosis and the cytoskeleton (Donaldson and Jackson, 2011; Jackson and Bouvet, 2014). Examination of an influence of Step on *Drosophila* cellularization led to the suggestion that Step reduced actin polymerization and myosin activity by decreasing levels of Rho1 through promotion of endocytic activity (Lee and Harris, 2013). Step has also been implicated in downregulating actomyosin activity to allow stretching of the dorsal epidermis during dorsal closure, and zebrafish cytohesins appear to play a similar role during epiboly (West et al., 2017). Prior to dorsal closure, during germband retraction, *step* mutants were observed to have myosin cables that appear more intense and continuous than in wild-type embryos (West et al., 2017). We did not observe obvious differences in myosin accumulation in *jub* embryos, but, even in *step* embryos, the differences in myosin were not dramatic. In imaginal discs, by contrast, clear differences in myosin accumulation, including abnormal and prominent myosin cables, were evident. Studies of Step during dorsal closure also revealed that its recruitment to cell junctions depends upon cytoskeletal tension, but the basis for this was unknown (West et al., 2017). Our observations have now

Journal of Cell Science (2019) 132, jcs224063. doi:10.1242/jcs.224063

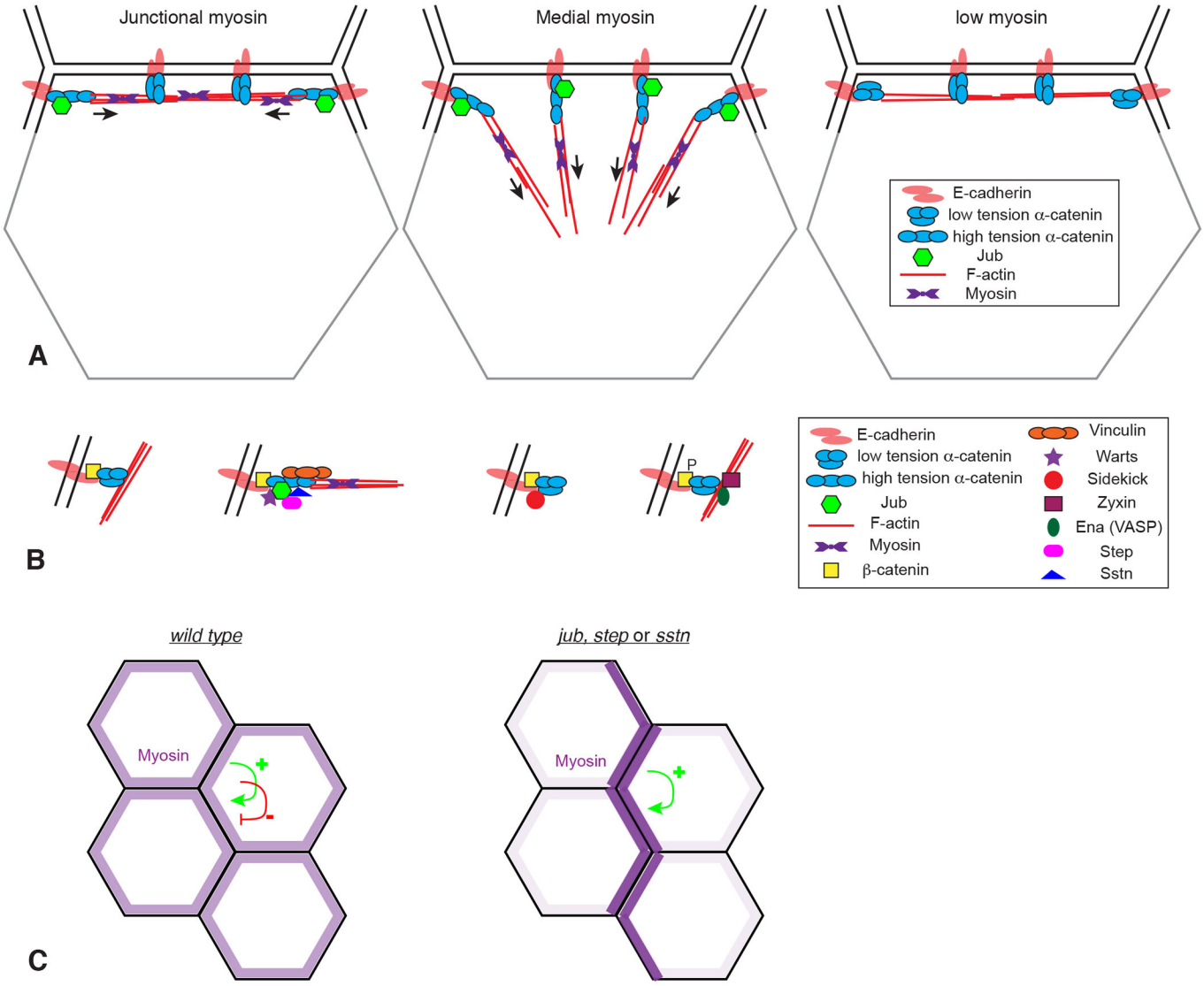

Fig. 7. Models for Jub localization and action at AJs. (A) Illustration of the hypothesis that formation of the high-tension conformation of α-catenin that binds Jub depends upon both the amount of tension (arrows) in actomyosin filaments (red lines) and its orientation relative to AJs. Jub binding requires tension applied perpendicular to the membrane. For simplicity, AJs are only shown along one side of the cell (black lines), not on other sides (gray lines). (B) Illustration of four different types of AJ complexes identified in wing imaginal disc cells at different locations around the cell circumference. (C) Illustration of how myosin distribution is altered in the absence of *jub*, *step* or *sstn*. Tension-dependent recruitment of myosin creates a positive-feedback loop, which, in the absence of the negative-feedback loop provided by Jub, Sstn and Step, we hypothesize results in accumulation of myosin in multicellular cables and depletion from other cell–cell junctions.

established a molecular mechanism for the tension-dependent recruitment of Step to AJs, by establishing that it depends upon Jub, which is recruited to AJs in a tension-dependent manner.

While this paper was in preparation, Razzell et al. (2018) described an analysis of *jub* embryos, with a focus on Jub localization and phenotypes during germband extension. Notably, they observed a significant increase in the formation and duration of multicellular rosettes during germband extension, consistent with the increased rosette formation we observed during dorsal closure. Also consistent with our observations, they observed tears between the dorsal epidermis and the amnioserosa. However, they interpreted *jub* phenotypes as evidence for a role of Jub in maintaining cell–cell adhesion during morphogenesis. Our linkage of Jub to Step suggests an alternative explanation, in which loss of Jub, and consequently loss of Step, leads to accumulation of excess tension at some cellular interfaces, which then may dissociate cell–cell junctions.

Jub, Sstn and Step appear to participate together in a negative-feedback loop: they are recruited to AJs by cytoskeletal tension and once at junctions they can downregulate cytoskeletal tension. However, absence of these proteins does not cause a general increase in myosin. Instead, it appears, at least in wing discs, that myosin is reorganized, from a relatively even distribution of junctional myosin to a very uneven distribution that includes prominent multicellular myosin cables along some junctions, while other junctions have little or no associated myosin. We propose that this shift could be explained by counterbalancing roles of positive- and negative-feedback loops that modulate myosin accumulation (Fig. 7C). Experimental observations have supported the existence of tension-dependent recruitment of myosin (Fernandez-Gonzalez et al., 2009; Pouille et al., 2009), and theoretical modeling of an active tension network that incorporates tension-dependent myosin recruitment can generate features of epithelial cell dynamics (Noll

et al., 2017). Tension-dependent recruitment of myosin generates a positive-feedback loop. Positive-feedback loops push a system towards extremes, and we suggest that the myosin distribution observed in the absence of Jub, Sstn or Step is what could be expected to occur if myosin localization were dominated by a positive-feedback loop – most myosin accumulates on a subset of junctions that experience and generate highest tension, and myosin becomes depleted from other junctions. The role of Jub–Step biomechanical signaling could thus be described as establishing a negative-feedback loop that generates evenly distributed myosin to counteract the positive-feedback loops that would otherwise generate uneven tension. Dynamic morphogenetic processes would require modulation of these feedback loops. For example, self-reinforcing tension and myosin recruitment could contribute to the formation of multicellular rosettes, but resolving these rosettes could require counteracting this tension-dependent myosin recruitment.

Our observations, together with those of Razzell et al. (2018), have identified a role for Jub in biomechanical signal transduction that is distinct from its role in cytoskeletal regulation of Hippo signaling. The role of Jub in Step recruitment to AJs suggests that it could be considered to act as a multifunctional adapter protein, which can recruit a variety of distinct proteins to AJs under tension to control cell behaviors, including Warts, to modulate Yki activity and cell proliferation, and Step, to modify cytoskeletal organization. The conserved role of zebrafish cytohesins in regulating tissue tension and myosin localization (West et al., 2017), together with the conservation of tension-dependent localization of vertebrate Ajuba family proteins to AJs (Chu et al., 2018; Ibar et al., 2018), raises the possibility that this pathway for biomechanical feedback could also play a key role in modulating cell behaviors in vertebrates.

MATERIALS AND METHODS

Drosophila genetics

Unless otherwise indicated, crosses were performed at 25°C. To create *jub* embryos, *Df(1)jubII FRT19A/FM7,sn twi-Gal4 UAS-GFP* females were crossed to *y w hs-FLP ovo^{D1} sn FRT19A* males. Larvae at 48–72 h after egg laying were heat-shocked for 1 h at 38°C to induce germline clones. Non-balancer adult female progeny were collected and crossed to sibling *FM7 sn twi-Gal4 UAS-GFP* males (for fixed imaging), *FM7 sn twi-Gal4 UAS-GFP; E-cad:GFP/+* males (for live imaging) or *FM7 Dfd-YFP* males (for embryonic viability analysis).

To drive expression in UAS-Gal4 experiments, we used *da-Gal4 Act-Gal4* in embryos, and *da-Gal4 Act-Gal4, nub-Gal4 UAS-dcr2* or *en-Gal4* in wing discs. For RNAi experiments, *en-Gal4 UAS-RFP UAS-dcr2*, *en-Gal4 UAS-GFP UAS-dcr2* or *nub-Gal4 UAS-dcr2* flies were crossed to RNAi lines and maintained at 29°C. RNAi transgenes used were *jub* [Vienna *Drosophila* Resource Center (VDRC) 38442], *Zyx* [National Institute of Genetics (NIG) 32018], *Vinc* (HMS02356), *step* (HMS00365), *step* (VDRC 34831), *sstn* (sstn#2), *ena* (VDRC 106484) and *Rok* (VDRC 104675). Both *step* RNAi lines gave similar results. *jub*, *sstn* and *Zyx* RNAi lines have been described and validated previously (Liu et al., 2015; Rauskolb et al., 2011). To increase myosin activity we used *UAS-sqh.EE* and *UAS-Rok.CA*. To monitor protein localization, we expressed Jub:GFP (Sabino et al., 2011), Vinc:RFP, Vinc:GFP (Klapholz et al., 2015), Sdk:GFP (FBst0060169), Zip:GFP (Buszczak et al., 2007), E-cad:GFP, sqh-sqh:mCherry, ex-lacZ (Hamaratoglu et al., 2006), UAS-YPet:Zyx (Colombelli et al., 2009), UAS-step:mCherry, UAS-step:GFP, UAS-sstn:mCherry, UAS-sstn:GFP (Liu et al., 2015).

Histology and imaging

Embryos were collected on apple juice agar plates with yeast, dechorionated with bleach, rinsed with water and then fixed using 1:1 4% paraformaldehyde fixative:heptane in a scintillation vial. Embryos were fixed with vigorous shaking on a flat-bed shaker for 15–20 min, devitellinized with methanol, rinsed with methanol and then rinsed with Ringers solution several times. Fixed embryos were either processed immediately for antibody staining, or stored in phosphate-buffered saline, pH7.4, plus 0.1% TritonX-100 and 1% BSA (PBT) at 4°C overnight before proceeding with staining protocols. To analyze F-actin in embryos, embryos were dechorionated, rinsed and then fixed in 1:1 8% paraformaldehyde fixative:heptane for 55 min. The fixed embryos were removed with a Pasteur pipette and transferred to an apple juice agar plate. All traces of fixative/heptane were removed and then double-stick tape was used to transfer the embryos to a Petri dish lid. The embryos were covered with PBT and hand-peeled using a sharp needle. Devitellenized embryos were transferred to an Eppendorf tube, rinsed with PBT and used for subsequent antibody stains. Fixation and staining of larval imaginal discs was performed essentially as described in Rauskolb and Irvine (2019). Wing discs were fixed in 4% paraformaldehyde for 12–15 min at room temperature. Primary antibodies used were mouse anti-β-galactosidase [1:200; Developmental Studies Hybridoma Bank (DSHB)], rat anti-E-cad (1:400; DCAD2, DSHB), mouse anti-Wg (1:800; DSHB), mouse anti-Ena (1:400; DSHB), rat anti-α-catenin (1:400; DSHB), rabbit anti-Y654 (1:100; Abcam, ab59430), mouse anti-Arm (1:200, DSHB) and rabbit anti-Yki (1:400) (Oh and Irvine, 2008). Secondary antibodies were from Jackson ImmunoResearch Laboratories and Invitrogen. DNA was stained using Hoechst 33342 (Life Technologies) and F-actin using phalloidin (1:10; Invitrogen Alexa Fluor 647). Confocal images were captured on a Leica SP8 confocal microscope. Confocal images to be directly compared were acquired under identical conditions, including tissue treatment, laser power and detector sensitivities, so that levels of expression would be directly comparable. This includes *nub-Gal4 UAS-Dcr2 UAS-step:Cherry* in wild type, *jub* RNAi, *Zyx* RNAi and *sstn* RNAi; *nub-Gal4 UAS-Dcr2 UAS-sstn:GFP* in wild type and *jub* RNAi; *nub-Gal4 UAS-Dcr2 UAS-step:GFP* in wild type and *Rok* RNAi; *nub-Gal4 UAS-Dcr2 UAS-sstn:GFP* in wild type and *Rok* RNAi; *en-Gal4 UAS-Dcr2 UAS-YPet:Zyx* in wild type, *jub* RNAi and *ena* RNAi; *en-Gal4 UAS-Dcr2 UAS-YPet:Zyx* in wild type and *Zyx* RNAi; *nub-Gal4 UAS-Dcr2 UAS-sstn:GFP* in wild type and *sstn* RNAi; *nub-Gal4 UAS-Dcr2 UAS-step:Cherry* in wild type and *step* RNAi; and *nub-Gal4 UAS-Dcr2 Jub:GFP* in wild type and *jub* RNAi.

For live imaging, embryos were collected on apple juice agar plates with yeast at 29°C, dechorionated with bleach and rinsed with water. They were then transferred to an apple juice agar plate and aligned with dorsal sides up. A coverslip with double-sided tape was used to stick them, and embryos were immediately covered with halocarbon oil 27 (Sigma-Aldrich). The coverslip was adhered via double-sided tape to a metal Leica FrameSlide with the polyethylene terephthalate membrane removed. The embryos in halocarbon oil were then covered with a YSI permeable membrane. Live imaging was conducted using an inverted spinning disc microscope, with images acquired every 5 min during dorsal closure.

For analysis of embryonic viability, eggs laid from GLC *jub* females were counted and transferred to an apple juice agar plate. Hatched larvae were scored for the presence (*jub* m-z+; n=197) or absence (*jub* m-z−; n=169) of Dfd-YFP. Expected ratio is 1:1. Less than 10% of the fertilized eggs did not hatch (n=17), but these could not be scored for Dfd-YFP. For a control, Oregon-R hatch rates were used (n=197; 14 of which did not hatch).

Image quantification and statistics

Junctional protein intensities were quantified in confocal stacks using Volocity software (PerkinElmer), using E-cad as a reference to define a junctional volume. Mean intensities were normalized to the mean E-cad intensity, and comparisons were made between anterior and posterior compartments (*en-Gal4*-driven transgenes), or between control and experimental discs treated and imaged under identical conditions (*nub-Gal4*-driven transgenes). Pearson's colocalization co-efficient was quantified using Volocity software, with Costes automatic thresholding. Line scans were performed using Fiji software (Schindelin et al., 2012) and averaged using Excel (Microsoft). Statistical tests were performed using GraphPad software (Prism). For pairwise comparisons of signal intensities, Student's *t*-tests were used, and for multiple comparisons of intensities of colocalization coefficients, one-way ANOVA was used. Comparisons of

ratios were performed on the log transform of the ratio. Kolmogorov–Smirnov tests were used for comparisons of mean junctional distributions.

Acknowledgements
We thank N. Brown, the DSHB, Bloomington *Drosophila* Stock Center, NIG and VDRC for antibodies and *Drosophila* stocks; Zhenru Zhou for initial observations of Sdk localization; Herve Alégot for assistance with live imaging of embryos; and Srividya Venkatramanan for validating *Vinc* RNAi lines.

Competing interests
The authors declare no competing or financial interests.

Author contributions
Conceptualization: C.R., K.D.I.; Methodology: C.R., K.D.I.; Investigation: C.R., E.C., F.M.; Writing - original draft: C.R., K.D.I.; Writing - review & editing: C.R., K.D.I.; Supervision: C.R., K.D.I.; Project administration: K.D.I.; Funding acquisition: K.D.I.

Funding
This research was supported by the National Institutes of Health [R01 GM121537 to K.D.I.]. Deposited in PMC for release after 12 months.

Supplementary information
Supplementary information available online at
http://jcs.biologists.org/lookup/doi/10.1242/jcs.224063.supplemental

References

Alégot, H., Markosian, C., Rauskolb, C., Yang, J., Kirichenko, E., Wang, Y.-C. and Irvine, K. D. (2019). Recruitment of Jub by alpha-catenin promotes Yki activity and Drosophila wing growth. *J. Cell Sci.* jcs.222018.

Astigarraga, S., Douthit, J., Tarnogorska, D., Creamer, M. S., Mano, O., Clark, D. A., Meinertzhagen, I. A. and Treisman, J. E. (2018). Drosophila Sidekick is required in developing photoreceptors to enable visual motion detection. *Development* **145**, dev158246.

Blankenship, J. T., Backovic, S. T., Sanny, J. S. P., Weitz, O. and Zallen, J. A. (2006). Multicellular rosette formation links planar cell polarity to tissue morphogenesis. *Dev. Cell* **11**, 459-470.

Brunet, T., Bouclet, A., Ahmadi, P., Mitrossilis, D., Driquez, B., Brunet, A.-C., Henry, L., Serman, F., Béalle, G., Ménager, C. et al. (2013). Evolutionary conservation of early mesoderm specification by mechanotransduction in Bilateria. *Nat. Commun.* **4**, 2821.

Buszczak, M., Paterno, S., Lighthouse, D., Bachman, J., Planck, J., Owen, S., Skora, A. D., Nystul, T. G., Ohlstein, B., Allen, A. et al. (2007). The Carnegie protein trap library: a versatile tool for Drosophila developmental studies. *Genetics* **175**, 1505-1531.

Byri, S., Misra, T., Syed, Z. A., Bätz, T., Shah, J., Boril, L., Glashauser, J., Aegerter-Wilmsen, T., Matzat, T., Moussian, B. et al. (2015). The triple-repeat protein anakonda controls epithelial tricellular junction formation in Drosophila. *Dev. Cell* **33**, 535-548.

Choi, W., Jung, K.-C., Nelson, K. S., Bhat, M. A., Beitel, G. J., Peifer, M. and Fanning, A. S. (2011). The single Drosophila ZO-1 protein Polychaetoid regulates embryonic morphogenesis in coordination with Canoe/afadin and Enabled. *Mol. Biol. Cell* **22**, 2010-2030.

Choi, W., Acharya, B. R., Peyret, G., Fardin, M.-A., Mège, R.-M., Ladoux, B., Yap, A. S., Fanning, A. S. and Peifer, M. (2016). Remodeling the zonula adherens in response to tension and the role of afadin in this response. *J. Cell Biol.* **213**, 243-260.

Chu, C.-W., Xiang, B., Ossipova, O., Ioannou, A. and Sokol, S. Y. (2018). The Ajuba family protein Wtip regulates actomyosin contractility during vertebrate neural tube closure. *J. Cell Sci.* **131**, jcs213884.

Colombelli, J., Besser, A., Kress, H., Reynaud, E. G., Girard, P., Caussinus, E., Haselmann, U., Small, J. V., Schwarz, U. S. and Stelzer, E. H. K. (2009). Mechanosensing in actin stress fibers revealed by a close correlation between force and protein localization. *J. Cell Sci.* **122**, 1665-1679.

Das Thakur, M., Feng, Y., Jagannathan, R., Seppa, M. J., Skeath, J. B. and Longmore, G. D. (2010). Ajuba LIM proteins are negative regulators of the Hippo signaling pathway. *Curr. Biol.* **20**, 657-662.

Donaldson, J. G. and Jackson, C. L. (2011). ARF family G proteins and their regulators: roles in membrane transport, development and disease. *Nat. Rev. Mol. Cell Biol.* **12**, 362-375.

Drees, B., Friederich, E., Fradelizi, J., Louvard, D., Beckerle, M. C. and Golsteyn, R. M. (2000). Characterization of the interaction between zyxin and members of the Ena/vasodilator-stimulated phosphoprotein family of proteins. *J. Biol. Chem.* **275**, 22503-22511.

Fernandez-Gonzalez, R., Simoes, S. D. M., Röper, J.-C., Eaton, S. and Zallen, J. A. (2009). Myosin II dynamics are regulated by tension in intercalating cells. *Dev. Cell* **17**, 736-743.

Franke, J. D., Montague, R. A. and Kiehart, D. P. (2005). Nonmuscle myosin II generates forces that transmit tension and drive contraction in multiple tissues during dorsal closure. *Curr. Biol.* **15**, 2208-2221.

Gaspar, P., Holder, M. V., Aerne, B. L., Janody, F. and Tapon, N. (2015). Zyxin antagonizes the FERM protein expanded to couple F-actin and Yorkie-dependent organ growth. *Curr. Biol.* **25**, 679-689.

Gates, J., Mahaffey, J. P., Rogers, S. L., Emerson, M., Rogers, E. M., Sottile, S. L., Van Vactor, D., Gertler, F. B. and Peifer, M. (2007). Enabled plays key roles in embryonic epithelial morphogenesis in Drosophila. *Development* **134**, 2027-2039.

Hamaratoglu, F., Willecke, M., Kango-Singh, M., Nolo, R., Hyun, E., Tao, C., Jafar-Nejad, H. and Halder, G. (2006). The tumour-suppressor genes NF2/Merlin and Expanded act through Hippo signalling to regulate cell proliferation and apoptosis. *Nat. Cell Biol.* **8**, 27-36.

Harris, T. J. C. and Tepass, U. (2010). Adherens junctions: from molecules to morphogenesis. *Nat. Rev. Mol. Cell Biol.* **11**, 502-514.

Heer, N. C. and Martin, A. C. (2017). Tension, contraction and tissue morphogenesis. *Development* **144**, 4249-4260.

Ibar, C., Kirichenko, E., Keepers, B., Enners, E., Fleisch, K. and Irvine, K. D. (2018). Tension-dependent regulation of mammalian Hippo signaling through LIMD1. *J. Cell Sci.* **131**, jcs214700.

Jackson, C. L. and Bouvet, S. (2014). Arfs at a glance. *J. Cell Sci.* **127**, 4103-4109.

Jurado, J., de Navascués, J. and Gorfinkiel, N. (2016). α-Catenin stabilises Cadherin-Catenin complexes and modulates actomyosin dynamics to allow pulsatile apical contraction. *J. Cell Sci.* **129**, 4496-4508.

Kale, G. R., Yang, X., Philippe, J.-M., Mani, M., Lenne, P.-F. and Lecuit, T. (2018). Distinct contributions of tensile and shear stress on E-cadherin levels during morphogenesis. *Nat. Commun.* **9**, 5021.

Kim, T.-J., Zheng, S., Sun, J., Muhamed, I., Wu, J., Lei, L., Kong, X., Leckband, D. E. and Wang, Y. (2015). Dynamic visualization of α-catenin reveals rapid, reversible conformation switching between tension states. *Curr. Biol.* **25**, 218-224.

Klapholz, B., Herbert, S. L., Wellmann, J., Johnson, R., Parsons, M. and Brown, N. H. (2015). Alternative mechanisms for talin to mediate integrin function. *Curr. Biol.* **25**, 847-857.

Koch, B. J., Ryan, J. F. and Baxevanis, A. D. (2012). The diversification of the LIM superclass at the base of the Metazoa increased subcellular complexity and promoted multicellular specialization. *PLoS ONE* **7**, e33261.

Leckband, D. E. and de Rooij, J. (2014). Cadherin adhesion and mechanotransduction. *Annu. Rev. Cell. Dev. Biol.* **30**, 291-315.

Lecuit, T. and Yap, A. S. (2015). E-cadherin junctions as active mechanical integrators in tissue dynamics. *Nat. Cell Biol.* **17**, 533-539.

Lee, D. M. and Harris, T. J. C. (2013). An Arf-GEF regulates antagonism between endocytosis and the cytoskeleton for Drosophila blastoderm development. *Curr. Biol.* **23**, 2110-2120.

Liu, J., Lee, D. M., Yu, C. G., Angers, S. and Harris, T. J. C. (2015). Stepping stone: a cytohesin adaptor for membrane cytoskeleton restraint in the syncytial Drosophila embryo. *Mol. Biol. Cell* **26**, 711-725.

Lye, C. M., Naylor, H. W. and Sanson, B. (2014). Subcellular localisations of the CPTI collection of YFP-tagged proteins in Drosophila embryos. *Development* **141**, 4006-4017.

Major, R. J. and Irvine, K. D. (2005). Influence of Notch on dorsoventral compartmentalization and actin organization in the Drosophila wing. *Development* **132**, 3823-3833.

Marie, H., Pratt, S. J., Betson, M., Epple, H., Kittler, J. T., Meek, L., Moss, S. J., Troyanovsky, S., Attwell, D., Longmore, G. D. et al. (2003). The LIM protein Ajuba is recruited to cadherin-dependent cell junctions through an association with alpha-catenin. *J. Biol. Chem.* **278**, 1220-1228.

Martin, A. C. and Goldstein, B. (2014). Apical constriction: themes and variations on a cellular mechanism driving morphogenesis. *Development* **141**, 1987-1998.

Nguyen, D. N., Liu, Y., Litsky, M. L. and Reinke, R. (1997). The sidekick gene, a member of the immunoglobulin superfamily, is required for pattern formation in the Drosophila eye. *Development* **124**, 3303-3312.

Noll, N., Mani, M., Heemskerk, I., Streichan, S. J. and Shraiman, B. I. (2017). Active tension network model suggests an exotic mechanical state realized in epithelial tissues. *Nat. Phys.* **13**, 1221-1226.

Oh, H. and Irvine, K. D. (2008). In vivo regulation of Yorkie phosphorylation and localization. *Development* **135**, 1081-1088.

Oldenburg, J., van der Krogt, G., Twiss, F., Bongaarts, A., Habani, Y., Slotman, J. A., Houtsmuller, A., Huveneers, S. and de Rooij, J. (2015). VASP, zyxin and TES are tension-dependent members of Focal Adherens Junctions independent of the α-catenin-vinculin module. *Sci. Rep.* **5**, 17225.

Pouille, P.-A., Ahmadi, P., Brunet, A.-C. and Farge, E. (2009). Mechanical signals trigger Myosin II redistribution and mesoderm invagination in Drosophila embryos. *Sci. Signal.* **2**, ra16.

Rauskolb, C. and Irvine, K. D. (2019). Localization of Hippo signaling components in drosophila by fluorescence and immunofluorescence. *Methods Mol. Biol.* **1893**, 61-73.

Rauskolb, C., Pan, G., Reddy, B. V. V. G., Oh, H. and Irvine, K. D. (2011). Zyxin links Fat signaling to the Hippo pathway. *PLoS Biol.* **9**, e1000624.

Rauskolb, C., Sun, S., Sun, G., Pan, Y. and Irvine, K. D. (2014). Cytoskeletal tension inhibits Hippo signaling through an Ajuba-Warts complex. *Cell* **158**, 143-156.

Razzell, W., Bustillo, M. E. and Zallen, J. A. (2018). The force-sensitive protein Ajuba regulates cell adhesion during epithelial morphogenesis. *J. Cell Biol.* **217**, 3715-3730.

Reinhard, M., Rüdiger, M., Jockusch, B. M. and Walter, U. (1999). VASP interaction with vinculin: a recurring theme of interactions with proline-rich motifs. *FEBS Lett.* **399**, 103-107.

Sabino, D., Brown, N. H. and Basto, R. (2011). Drosophila Ajuba is not an Aurora-A activator but is required to maintain Aurora-A at the centrosome. *J. Cell Sci.* **124**, 1156-1166.

Schimizzi, G. V. and Longmore, G. D. (2015). Ajuba proteins. *Curr. Biol.* **25**, R445-R446.

Schindelin, J., Arganda-Carreras, I., Frise, E., Kaynig, V., Longair, M., Pietzsch, T., Preibisch, S., Rueden, C., Saalfeld, S., Schmid, B. et al. (2012). Fiji: an open-source platform for biological-image analysis. *Nat. Methods* **9**, 676-682.

Schulte, J., Tepass, U. and Auld, V. J. (2003). Gliotactin, a novel marker of tricellular junctions, is necessary for septate junction development in Drosophila. *J. Cell Biol.* **161**, 991-1000.

Smith, M. A., Blankman, E., Gardel, M. L., Luettjohann, L., Waterman, C. M. and Beckerle, M. C. (2010). A zyxin-mediated mechanism for actin stress fiber maintenance and repair. *Dev. Cell* **19**, 365-376.

Smith, M. A., Blankman, E., Deakin, N. O., Hoffman, L. M., Jensen, C. C., Turner, C. E. and Beckerle, M. C. (2013). LIM domains target actin regulators paxillin and zyxin to sites of stress fiber strain. *PLoS ONE* **8**, e69378.

Tamada, M. and Zallen, J. A. (2015). Square cell packing in the Drosophila embryo through spatiotemporally regulated EGF receptor signaling. *Dev. Cell* **35**, 151-161.

Uemura, A., Nguyen, T.-N., Steele, A. N. and Yamada, S. (2011). The LIM domain of zyxin is sufficient for force-induced accumulation of zyxin during cell migration. *Biophys. J.* **101**, 1069-1075.

West, J. J., Zulueta-Coarasa, T., Maier, J. A., Lee, D. M., Bruce, A. E. E., Fernandez-Gonzalez, R. and Harris, T. J. C. (2017). An actomyosin-Arf-GEF negative feedback loop for tissue elongation under stress. *Curr. Biol.* **27**, 2260-2270.e5.

Yao, M., Qiu, W., Liu, R., Efremov, A. K., Cong, P., Seddiki, R., Payre, M., Lim, C. T., Ladoux, B., Mège, R.-M. et al. (2014). Force-dependent conformational switch of α-catenin controls vinculin binding. *Nat. Commun.* **5**, 4525.

Yap, A. S., Duszyc, K. and Viasnoff, V. (2017). Mechanosensing and mechanotransduction at cell-cell junctions. *Cold Spring Harb. Perspect. Biol.* **10**, a028761.

Yonemura, S., Wada, Y., Watanabe, T., Nagafuchi, A. and Shibata, M. (2010). alpha-Catenin as a tension transducer that induces adherens junction development. *Nat. Cell Biol.* **12**, 533-542.

Supplemental Figures

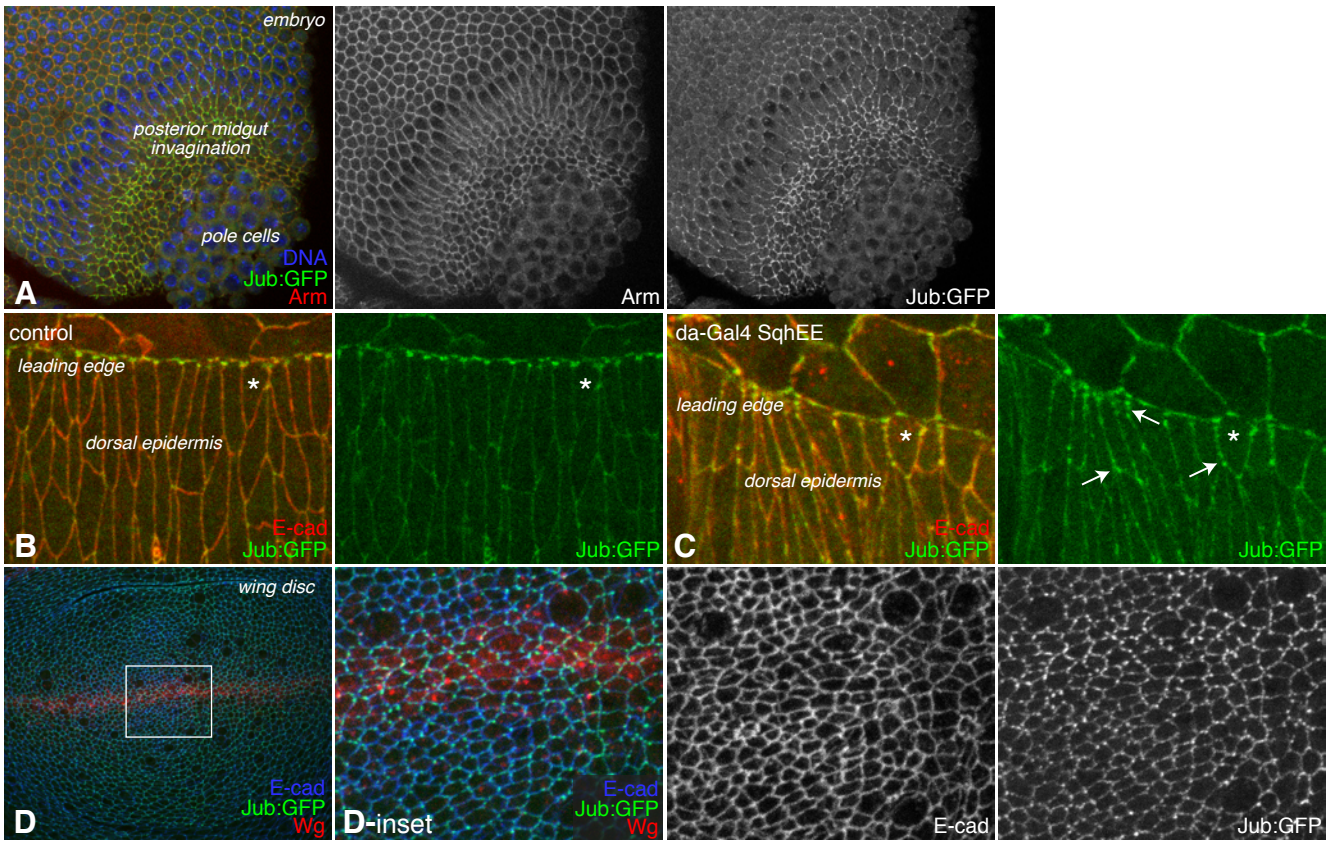

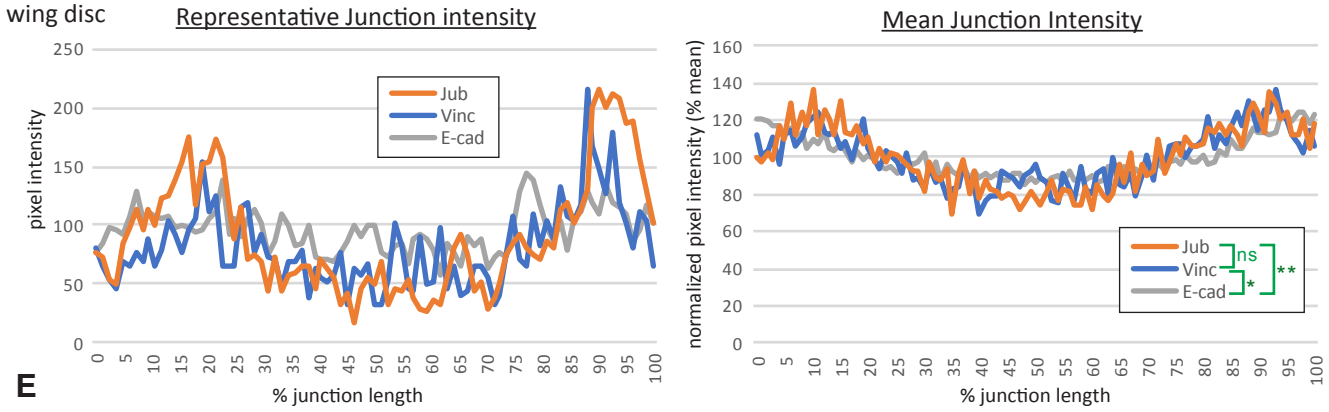

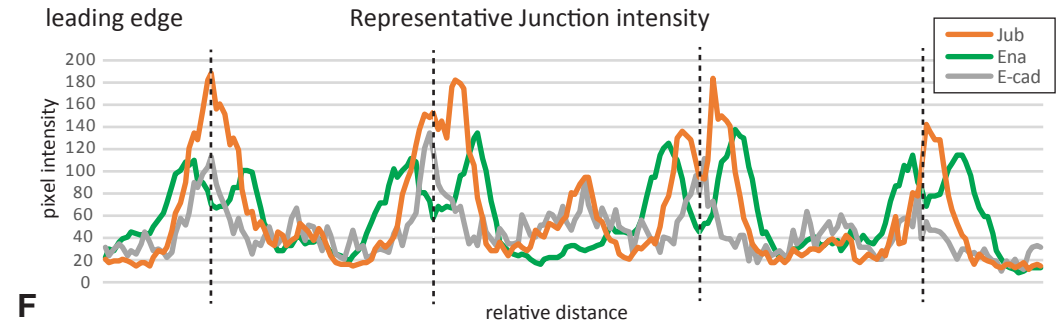

Figure S1. Jub localization at different stages of development

A) Localization of Jub:GFP (green/white) in posterior mid-gut invagination, compared to DNA (blue) and Armadillo (Arm, ß-catenin, red/white), B) Jub:GFP (green) and E-cad (red) in dorsal epidermis and leading edge cells during dorsal closure. C) Jub:GFP (green) and E-cad (red) in dorsal epidermis and leading edge cells during dorsal closure in an embryo expressing activated-myosin (UAS-Sqh.EE) under da-Gal4 control. Junctional localization of Jub:GFP is increased, e.g. compare cell labelled by asterisk in B and C. Arrows point to some sites with elevated Jub. D) Wing disc expressing Jub:GFP (green/white) stained for expression of Wg (red) and E-cad (blue/white). E) Left side: Line scan of signal intensity for Jub, Vinc and E-cad along a single junction between wing disc cells (as in Fig. 2A). Right side: Average intensity along wing disc junctions, normalized to the mean junction intensity, and plotted as percent junction length, for Jub (n=42), Vinc (n=25), and E-cad (n=74). E-cad intensity tends to be slightly higher near vertices and lower in the middle of the junction. Bright puncta of Jub and Vinc occur preferentially near vertices, but this preference is not absolute, and the distance of puncta from vertices varies. This is reflected in a slight relative increase in Jub and Vinc around 10-20 and 80-90 percent junction length. Kolmogorov-Smirnov tests of the significance of the difference between distributions identifies a difference between Vinc and E-cad, and between Jub and E-cad, but not between Vinc and Jub. ns, $P>0.05$, * $P\leq0.05$, ** $P\leq0.01$. F) Line scan of signal intensity for Jub, Ena and E-cad along the leading edge (as in Fig. 2C). Dashed lines indicate approximate locations of junctions between dorsal leading edge cells.

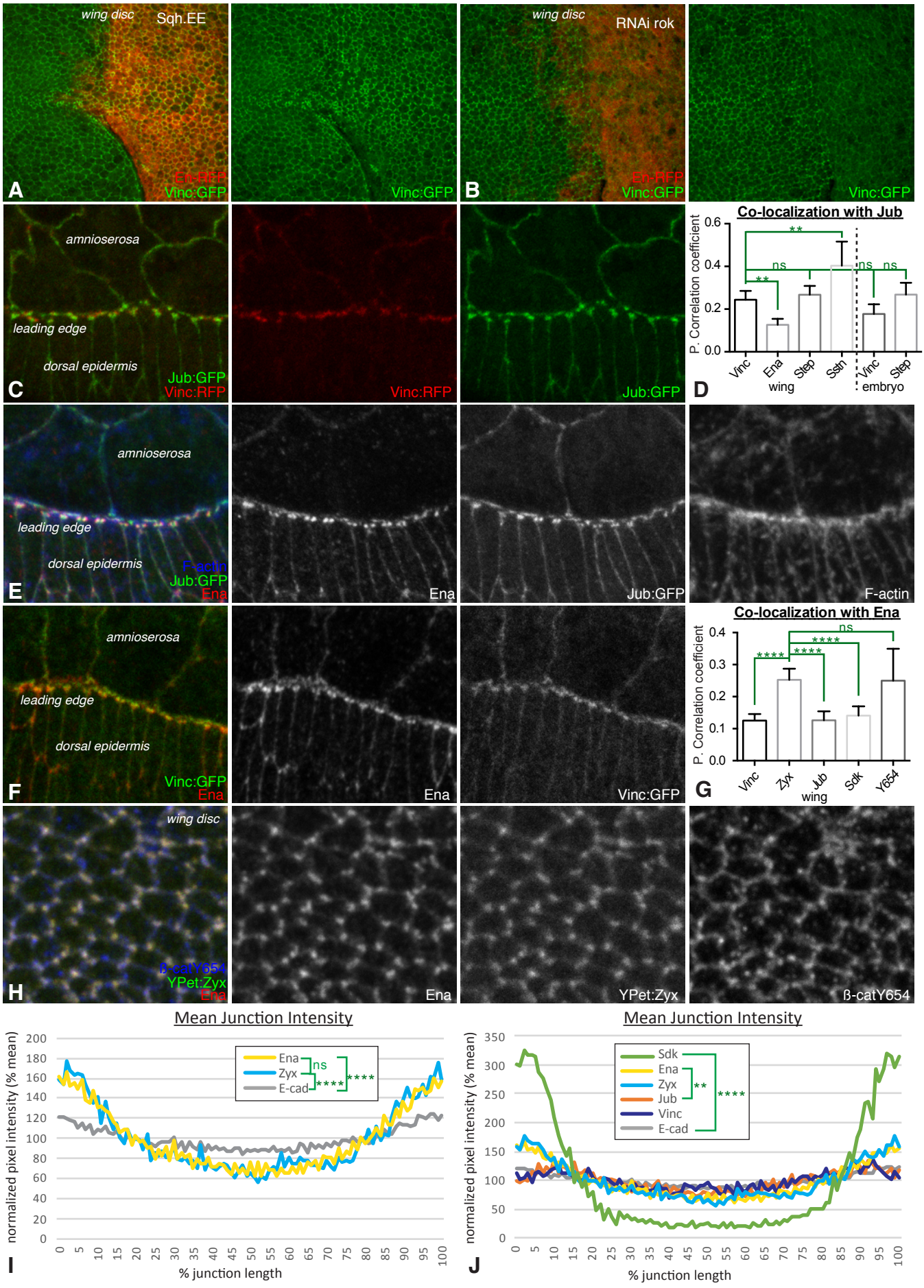

Journal of Cell Science • Supplementary information

Figure S2. Localization of AJ complex proteins

A,B) Wing discs expressing Vinc:GFP and in posterior cells under en-Gal4 control UAS-RFP (red) and (A) UAS-Sqh.EE or (B) UAS-RNAi-rok. C,E,F) Leading edge cells during dorsal closure, comparing expression of (C) Vinc:RFP and Jub:GFP, (E) Ena (red/white), Jub:GFP (green/white) and F-actin (blue/white), (F) Ena (red/white) and Vinc:GFP (green/white). D,G) Quantitation of Pearson's co-localization coefficient between Jub and the indicated proteins (D) and between Ena and the indicated proteins (G). For Jub (D), we compare the extent of co-localization between Jub and Vinc in wing discs with the other proteins indicated, only for Ena and Sstn is the extent of co-localization significantly different. For Ena (G), we compare the extent of co-localization with Zyx, which significantly differs from co-localization with Vinc, Jub, and Sdk, but not Y654. H) Wing disc cells expressing UAS-YPet:Zyx under da-Gal4 and act-Gal4 control, stained for Ena (red/white) and pY654-ß-cat. I,J) Average intensities along wing disc junctions, normalized to the mean junction intensity, and plotted as percent junction length, for Ena (n=49), Zyx (n=16) and E-cad (n=74) (I), or Ena, Zyx, E-cad, Jub (n=42), Vinc (n=25), and Sdk (n=17) (J). Distinct plots are provided with differences in scaling, as Sdk is much more tightly localized along junctions as compared to other proteins. A Kolmogorov-Smirnov tests of the significance of the difference between distributions identifies differences between Ena and E-cad, between Zyx and E-cad, between Ena and Jub, and between Sdk and E-cad, but not between Ena and Zyx. ns, $P>0.05$, ** $P\leq0.01$, **** $P\leq0.0001$.

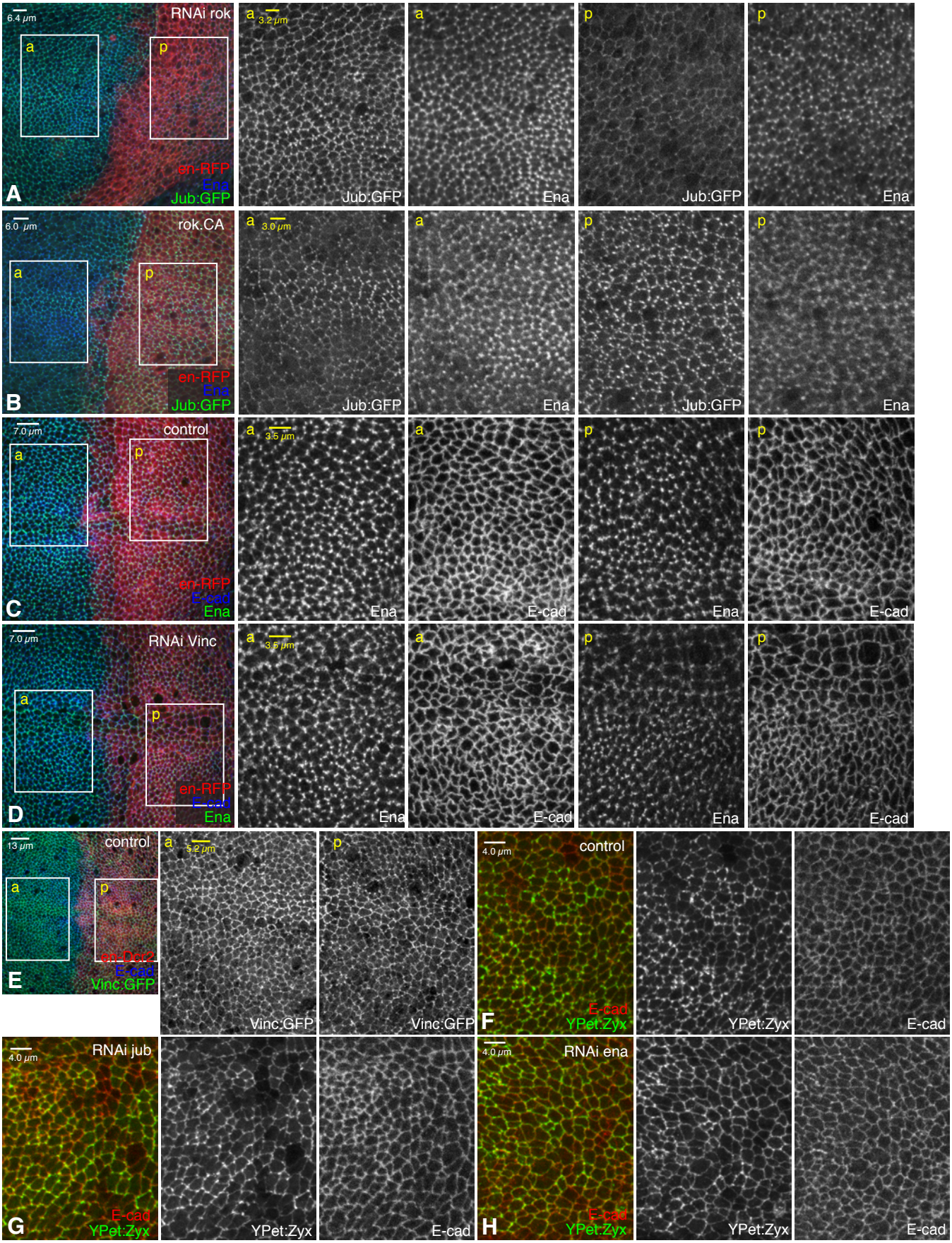
6.4 μm
RNAi rok
a
p
en-RFP
Ena
Jub:GFP
A
a
3.2 μm
Jub:GFP
a
Ena
p
Jub:GFP
p
Ena
6.0 μm
rok.CA
a
p
en-RFP
Ena
Jub:GFP
B
a
3.0 μm
Jub:GFP
a
Ena
p
Jub:GFP
p
Ena
7.0 μm
control
a
p
en-RFP
E-cad
Ena
C
a
3.5 μm
Ena
a
E-cad
p
Ena
p
E-cad
7.0 μm
RNAi Vinc
a
p
en-RFP
E-cad
Ena
D
a
3.5 μm
Ena
a
E-cad
p
Ena
p
E-cad
13 μm
control
a
p
en-Dcr2
E-cad
Vinc:GFP
E
a
5.2 μm
Vinc:GFP
p
Vinc:GFP
4.0 μm
control
E-cad
YPet:Zyx
F
YPet:Zyx
E-cad
4.0 μm
RNAi jub
E-cad
YPet:Zyx
G
YPet:Zyx
E-cad
4.0 μm
RNAi ena
E-cad
YPet:Zyx
H
YPet:Zyx
E-cad

Figure S3. Influence of tension on Jub and Ena, and independent junctional localization of Ena and Zyx

Wing imaginal discs in which UAS transgenes were expressed in posterior cells (red) under *en-Gal4* control to assess potential requirements for localization of AJ complex proteins. In A-E, panels to the right show higher magnification images of the anterior (a) or posterior (p) boxes. A) RNAi of rok reduces Jub (green/white) junctional localization, but not Ena (blue/white). B) Activation of Rok (UAS-rok.CA) increases Jub (green/white) junctional localization, but not Ena (blue/white). C) Control wing disc stained for Ena (green/white) and E-cad (blue/white). D) RNAi of Vinc does not affect Ena (green/white) localization. E) Control wing disc expressing Vinc:GFP (green/white) and stained for E-cad (blue/white). F-H) Posterior region of wing discs expressing UAS-YPet:Zyx (green) and (F) control, , (G) UAS-RNAi-jub, (H) UAS-RNAi-ena stained for E-cad (red).

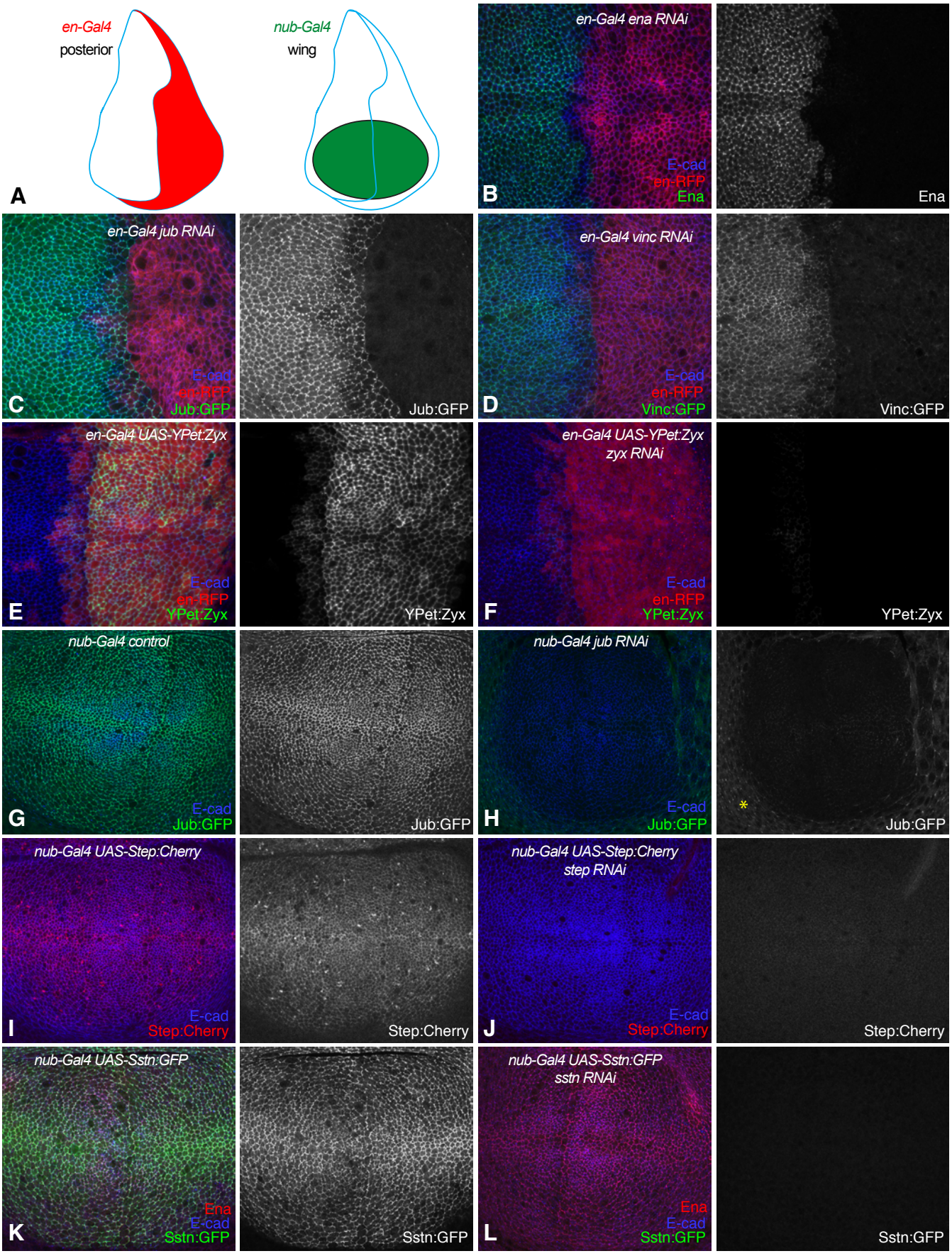

Figure S4. Effectiveness of RNAi

A) Schematics illustrating approximate expression domains of en-Gal4 and nub-Gal4 within the wing imaginal disc. B-F) Confocal images of wing imaginal discs expressing UAS transgenes in P cells under en-Gal4 control, stained for E-cad (blue), and: B) UAS-RNAi ena and stained for Ena (green/white). C) Jub:GFP (green/white) and UAS-RNAi jub. D) Vinc:GFP (green/white) and UAS-RNAi Vinc. E) UAS-YPet:Zyx (green/white). F) UAS-YPet:Zyx (green/white) and UAS-RNAi Zyx. G-L) Confocal images of wing imaginal discs expressing UAS transgenes in wing cells under nub-Gal4 control, stained for E-cad (blue), and: G) Jub:GFP (green/white). H) Jub:GFP (green/white) and UAS-RNAi jub. Proximal signal (asterisk) comes from outside the nub-Gal4 expression domain, which is reduced in size due to *jub* RNAi. I) UAS-Step:Cherry (red/white). J) UAS-Step:Cherry (red/white) and UAS-RNAi step. K) UAS-Sstn:GFP (green/white). L) UAS-Sstn:GFP (green/white) and UAS-RNAi sstn.

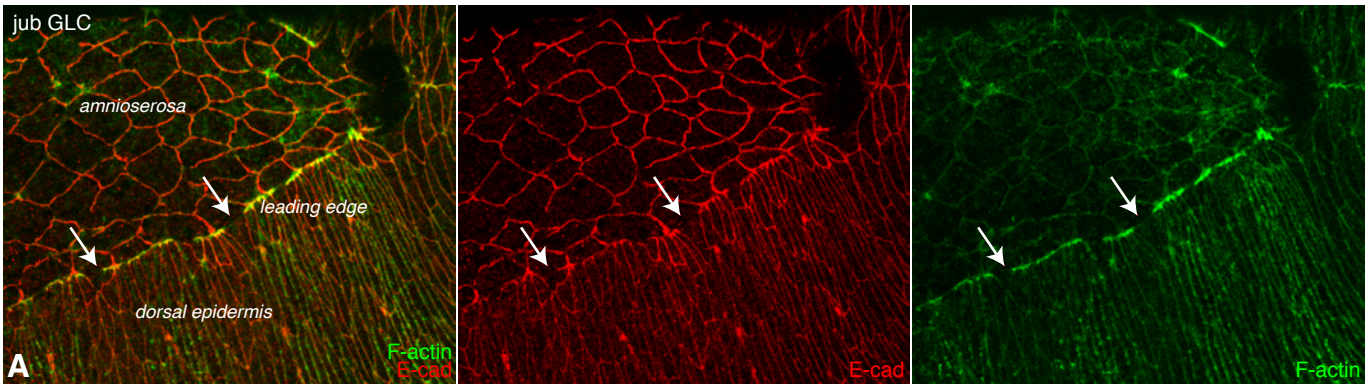

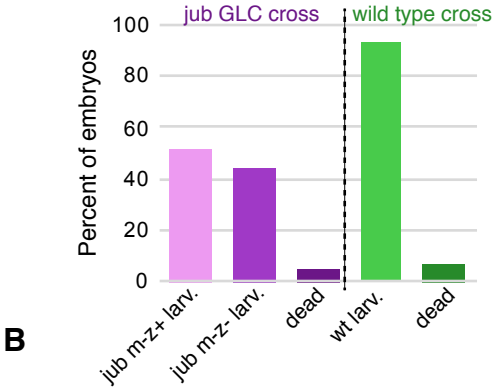

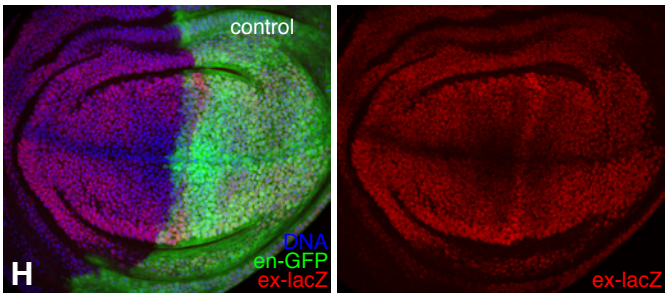

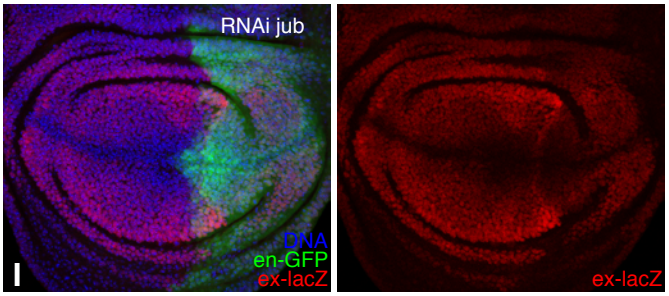

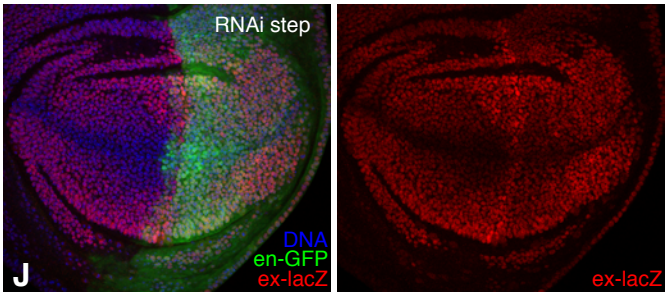

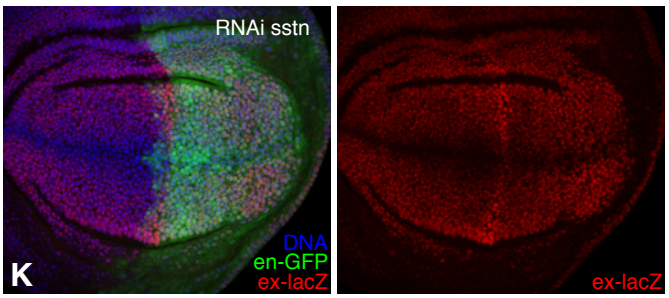

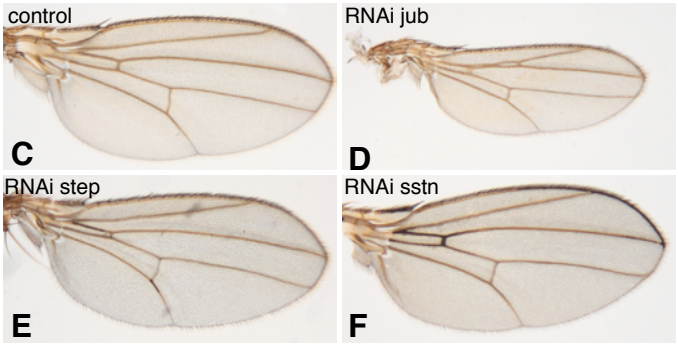

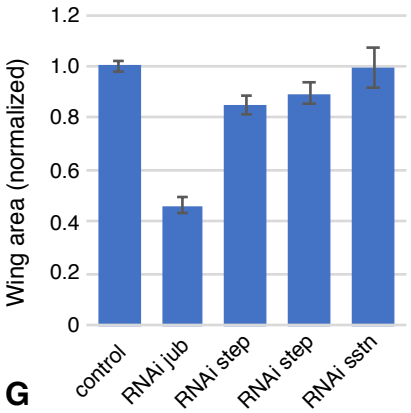

Figure S5. Phenotypes of *jub* and *step*

A) Example of *jub* embryo with gaps (highlighted by arrows) in the leading edge cable revealed by staining for E-cad and F-actin. B) Quantitation of embryonic viability in a cross of females with *jub* germline clones to FM7, Dfd-YFP males (magenta) and in wild-type (Oregon-R) control (green). The germline clone cross generates *jub*$^{-}$ males (m-z-, n=169)*, and jub*$^{-}$ */ FM7 Dfd-YFP* females (m-z+, n=197). The Dfd-YFP marker can be reliably scored in live embryos and larvae, but not in dead embryos (n=17); as an upper limit, if all dead embryos are m-z- then 9% (17/186) of progeny are embryonic lethal. In the control 7% (14/197) of offspring died during embryogenesis. C-F) Adult wings from flies expressing nub-Gal4 and (C) control, (D) UAS-RNAi-jub, (E) UAS-RNAi-step, (F) UAS-RNAi-sstn. G) Histogram showing wing size, normalized to control wings, in flies expressing the indicated UAS-RNAi lines. N=10 (control, jub, step HMS), 13 (step vdrc), or 14 (sstn). error bars indicate s.d. H-K) Wing discs expressing RNAi lines in posterior cells (green) under en-Gal4 control, and stained for ex-lacZ (red) and DNA(blue), and expressing, H) control, I) UAS-RNAi-jub, J) UAS-RNAi-step, K) UAS-RNAi-sstn.

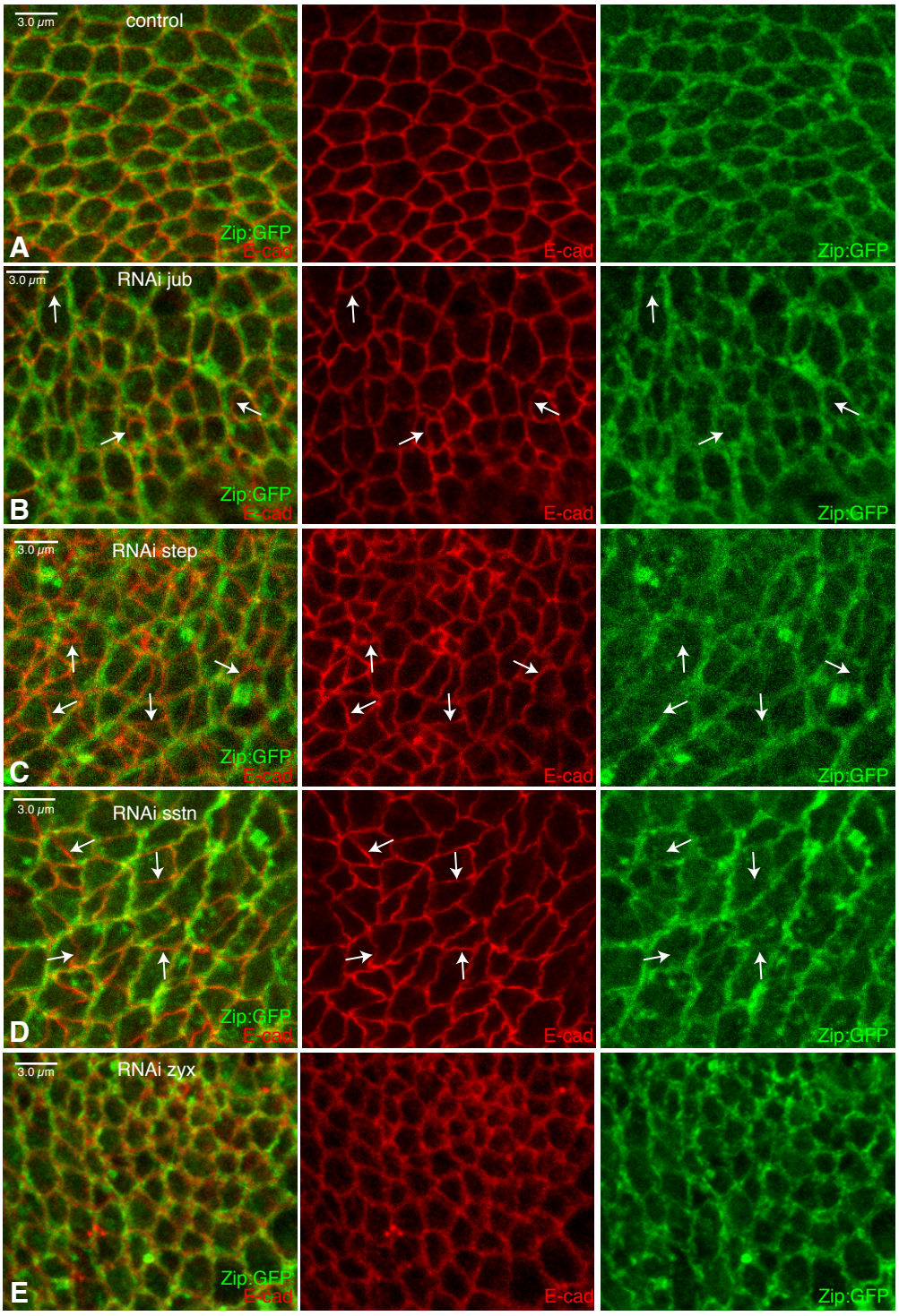

Figure S6. Influence of *jub*, *step, sstn* and *zyx* on wing disc epithelia

Wing disc cells expressing RNAi lines under *en-Gal4* control, stained for E-cad (red) and also expressing Zip:GFP (green). A) control. B) UAS-RNAi-jub. C) UAS-RNAi-step. D) UAS-RNAi-sstn. E) UAS-RNAi-Zyx. Arrows highlight examples of AJ with little or no associated myosin (Zip:GFP).

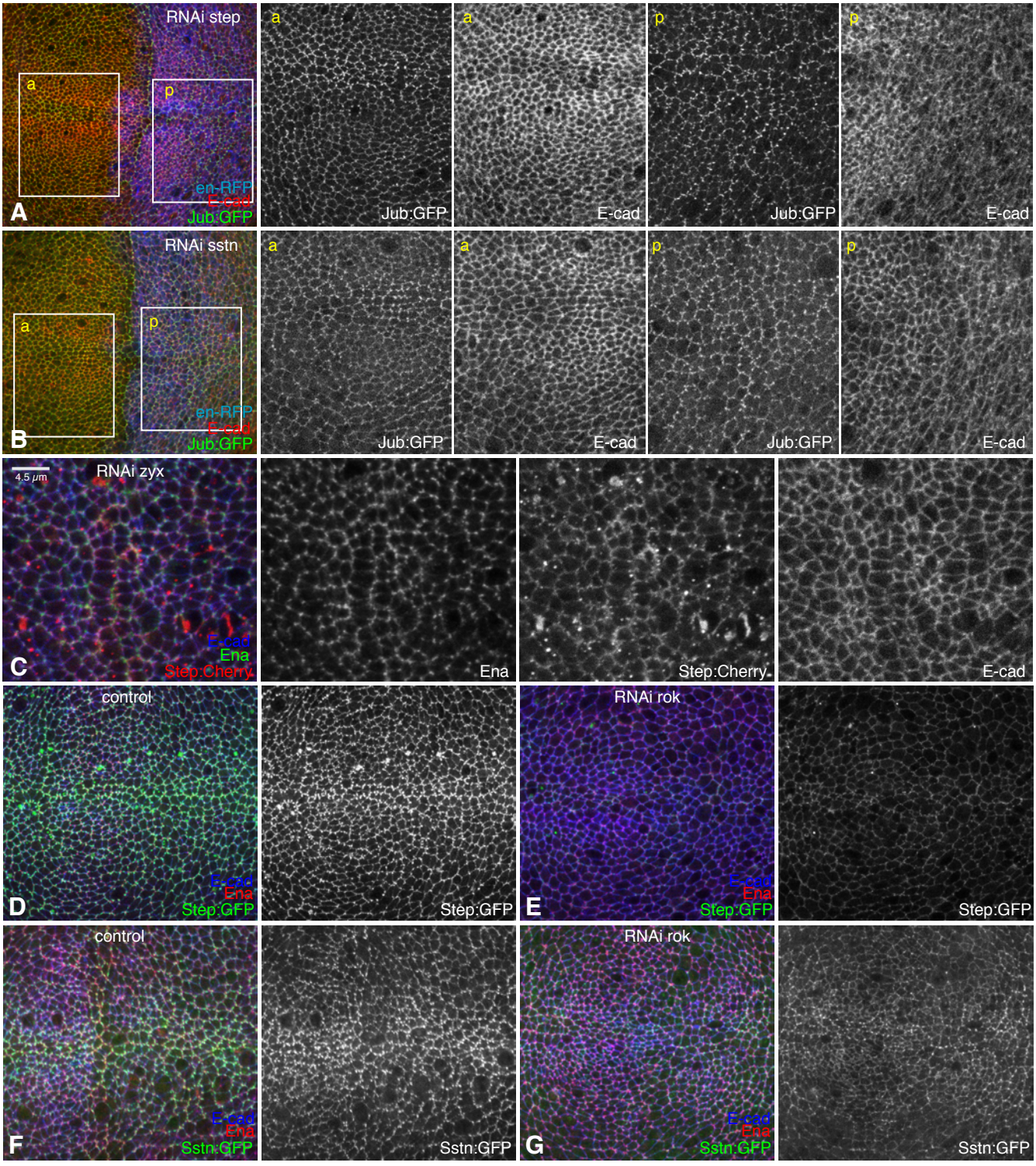
RNAi step
a
p
en-RFP
E-cad
Jub:GFP
A
a
Jub:GFP
a
E-cad
p
Jub:GFP
p
E-cad
RNAi sstn
a
p
en-RFP
E-cad
Jub:GFP
B
a
Jub:GFP
a
E-cad
p
Jub:GFP
p
E-cad
4.5 μm
RNAi zyx
E-cad
Ena
Step:Cherry
C
Ena
Step:Cherry
E-cad
control
E-cad
Ena
Step:GFP
D
Step:GFP
RNAi rok
E-cad
Ena
Step:GFP
E
Step:GFP
control
E-cad
Ena
Sstn:GFP
F
Sstn:GFP
RNAi rok
E-cad
Ena
Sstn:GFP
G
Sstn:GFP

Figure S7. Regulation of Step and Sstn localization in wing discs, and lack of influence of Step and Sstn on Jub

Wing discs expressing UAS-RNAi lines either in posterior cells (marked by UAS-RFP, blue) under *en-Gal4* control (A,B), or in all wing cells under *nub-Gal4* control (C-G), stained for expression of E-cad (red/white/blue). A) RNAi-*step* does not lead to loss of Jub (green/white). B) RNAi-*sstn* does not lead to loss of Jub (green/white). C) UAS-RNAi-Zyx does not remove UAS-Step:Cherry (red/white) from cell membranes. D) Control expressing UAS-Step:GFP. E) UAS-RNAi-rok results in a decrease in UAS-Step:GFP levels. F) Control expressing UAS-Sstn:GFP. G) UAS-RNAi-rok slightly reduces UAS-Sstn:GFP. Identical imaging conditions were used for (D) and (E), and for (F) and (G) and thus they are directly comparable.

Supplemental Movies

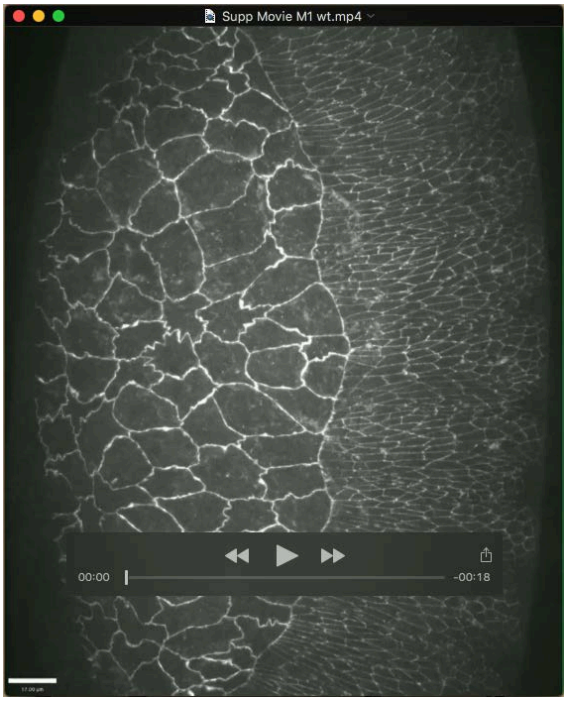

Movie 1. Dorsal closure in a *wild-type* embryo. Dorsal epidermal cells of a wild-type embryo, outlined by E-cad:GFP. Time is at upper right, and a scale bar is at lower left.

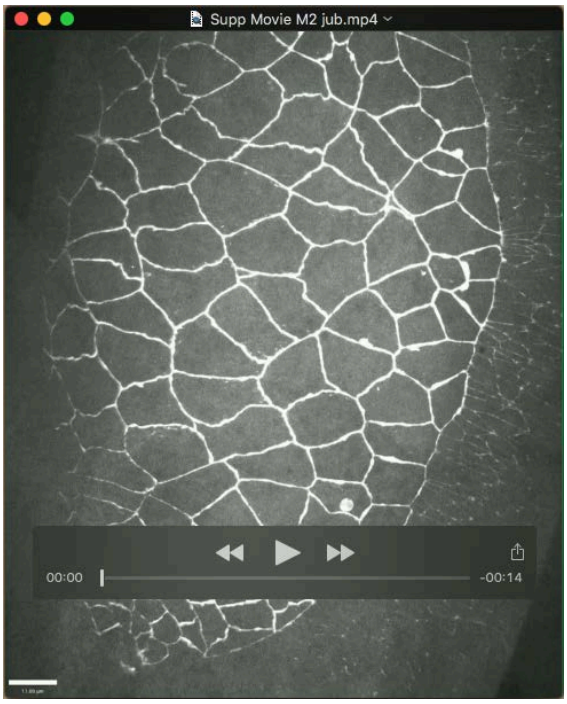

Movie 2. Dorsal closure in a *jub* embryo. Dorsal epidermal cells of a *jub* germ line clone embryo, outlined by E-cad:GFP. Time is at upper right, and a scale bar is at lower left.